arXiv:1405.5142v1 [astro-ph.SR] 20 May 2014

DISTRIBUTIONS OF SHORT-LIVED RADIOACTIVE NUCLEI PRODUCED BY YOUNG EMBEDDED STAR CLUSTERS

Fred C. Adams[1,2], Marco Fatuzzo[3], and Lisa Holden[4]

[1]*Physics Department, University of Michigan, Ann Arbor, MI 48109*

[2]*Astronomy Department, University of Michigan, Ann Arbor, MI 48109*

[3]*Physics Department, Xavier University, Cincinatti, OH 45255*

[4]*Department of Mathematics, Northern Kentucky University, Highland Heights, KY 41099*

ABSTRACT

Most star formation in the Galaxy takes place in clusters, where the most massive members can affect the properties of other constituent solar systems. This paper considers how clusters influence star formation and forming planetary systems through nuclear enrichment from supernova explosions, where massive stars deliver short-lived radioactive nuclei (SLRs) to their local environment. The decay of these nuclei leads to both heating and ionization, and thereby affects disk evolution, disk chemistry, and the accompanying process of planet formation. Nuclear enrichment can take place on two spatial scales: [1] Within the cluster itself ($\ell \sim 1$pc), the SLRs are delivered to the circumstellar disks associated with other cluster members. [2] On the next larger scale ($\ell \sim 2 - 10$pc), SLRs are injected into the background molecular cloud; these nuclei provide heating and ionization to nearby star-forming regions, and to the next generation of disks. For the first scenario, we construct the expected distributions of radioactive enrichment levels provided by embedded clusters. Clusters can account for the SLR mass fractions inferred for the early Solar Nebula, but typical SLR abundances are lower by a factor of ~ 10. For the second scenario, we find that distributed enrichment of SLRs in molecular clouds leads to comparable abundances. For both the direct and distributed enrichment processes, the masses of ^{26}Al and ^{60}Fe delivered to individual circumstellar disks typically fall in the range $10 - 100 pM_\odot$ (where $1 pM_\odot = 10^{-12} M_\odot$). The corresponding ionization rate due to SLRs typically falls in the range $\zeta_{SLR} \sim 1 - 5 \times 10^{-19}$ sec^{-1}. This ionization rate is smaller than that due to cosmic rays, $\zeta_{CR} \sim 10^{-17}$ sec^{-1}, but will be important in regions where cosmic rays are attenuated (e.g., disk mid-planes).

Subject headings: stars: formation — planetary systems: formation — open clusters and associations: general

1. Introduction

Within our Galaxy, most star formation takes place within embedded stellar clusters, where these systems display a wide range of sizes and other properties (e.g, Lada & Lada 2003; Porras et al. 2003; Allen et al. 2007). These background environments can influence the evolution and properties of planetary systems forming within them through a variety of processes (Hester & Desch 2005; Looney et al. 2006; Levison et al. 2010; Adams 2010; Pfalzner 2013), including dynamical scattering by other stellar members (Adams & Laughlin 2001; Adams et al. 2006; Malmberg et al. 2007), evaporation of circumstellar disks by radiation from massive stars (Störzer & Hollenbach 1999; Adams et al. 2004), accretion of cluster gas onto the disks (Throop & Bally 2008), and the injection of short-lived radioactive nuclei (hereafter SLRs) into circumstellar disks and/or collapsing regions (Cameron 1993; Meyer & Clayton 2000; Ouellette et al. 2007). This paper focuses on this latter issue of nuclear enrichment. In particular, we construct probability distributions for the abundances of SLRs that are expected to be delivered to forming solar systems in cluster environments, as well as to the larger, surrounding regions in molecular clouds.

Previous work regarding nuclear enrichment has focused on two related but somewhat different goals. The first approach considers the largest spatial scales, where a great deal of work has been carried out to estimate the steady state production rates and abundances of SLRs in the Galaxy (Timmes et al. 1995a,b). For example, gamma-ray emission due to the radioactive decay of ^{26}Al has been observed for the 1808.65 keV line (Diehl et al. 2006; Smith 2003). Since the Galaxy does not appreciably attenuate such emission, it can be used to determine the galactic inventory of ^{26}Al; the abundances of other nuclear species can be assessed in similar fashion. Such measurements, in conjunction with stellar evolution calculations that determine nuclear yields (Woosley & Weaver 1995; Woosley et al. 2002; Rauscher et al. 2002; Limongi & Chieffi 2006), can then be used to estimate (or constrain) the Galactic star formation rate. In an similar vein, gamma-ray observations have also measured the emission due to decay of ^{60}Fe. By comparing the ratio of line strengths, one can test whether or not the inferred abundances of ^{60}Fe and ^{26}Al are consistent with predictions of stellar nucleosynthesis models (Prantzos 2004). The results are consistent at the factor-of-two level, which is comparable to the uncertainties in these quantities.

On smaller scales, our own Solar System was apparently enriched in SLRs during its early formative stages. A great deal of previous work has been carried out to explain the nuclear abundance patterns deduced from meteoritic studies. Evidence for the enrichment of ^{26}Al is well-established, and the proposal that such enrichment arises from nearby supernovae dates back to Cameron & Truran (1977), or even further. Although ^{26}Al is readily produced in supernovae, it can also be synthesized through spallation. More recently, meteoritic

evidence for live ^{60}Fe in the early solar system has been reported (Tachibana et al. 2006) and bolsters the case for supernova enrichment of SLRs (because ^{60}Fe can only be produced via stellar nucleosynthesis). In contrast to the case of ^{26}Al, however, the evidence for ^{60}Fe is controversial and elusive (Moynier et al. 2011). For example, the inferred abundances can be biased for low count rates, such as those found for ^{60}Fe (Telus et al. 2012). On the other hand, a recent study (Mishra & Goswami 2014) concludes that the two SLRs ^{26}Al and ^{60}Fe were co-injected into the early solar system from same stellar source. In any case, for the purposes of this paper, we consider the two nuclear species to be on a nearly equal footing. As discussed below, stellar evolution models predict comparable abundances for ^{26}Al and ^{60}Fe, and both species are expected to make substantial contributions to ionization and heating within enriched regions.

The apparent need for nuclear enrichment of the early Solar System places constraints on the birth environment of the solar system (Adams & Laughlin 2001; Hester & Desch 2005; Williams & Gaidos 2007; Gounelle & Meibom 2008; Gounelle et al. 2009; Adams 2010; Pfalzner 2013; Dauphas & Chaussidon 2011). The requirement that the Sun is born near a high mass progenitor favors the scenario where the Sun is formed within a large cluster, but such environments can also lead to disruption through dynamical scattering interactions (Adams et al. 2006; Malmberg et al. 2007; Dukes & Krumholz 2012) and intense radiation fields (Fatuzzo & Adams 2008; Holden et al. 2011; Thompson 2013). For the nuclear enrichment of our Solar System, these previous studies (along with many others, including Looney et al. 2006; Williams 2010; Parker et al. 2014) suggest that the probability of enrichment is low, perhaps 1–10%, where the estimated value depends on how the accounting is done. On the other hand, observations of accreted extrasolar asteroids in white dwarf atmospheres indicate that the elevated levels of ^{26}Al inferred for the formation of own Solar System are not abnormal (Jura et al. 2013).

Building upon the aforementioned previous work, this paper considers nuclear enrichment on an intermediate scale. Instead of focusing on the enrichment of our own Solar System, we consider the general problem of determining the distribution of enrichment levels that are expected for the whole population of forming stars within a cluster. We also consider nuclear enrichment on the next larger scale of the molecular cloud, but do not focus on the scale of the Galaxy. Nonetheless, this work informs the larger scale picture, as the results must be consistent with galaxy-wide estimates for nuclear production and the accompanying star formation rate. On the scale of our own Solar System, this work constrains the probability of attaining the levels of nuclear enrichment inferred for our own solar nebula.

The decay of SLRs is important for star and planet formation for two related reasons: ionization and heating. The nuclear decay products are highly energetic, with $E \sim 1$ MeV.

As these particles, mainly photons and positrons, interact with their immediate environment, their energy cascades down to photons of lower energy. After the cascade proceeds to sufficiently low energy, the remaining photons interact with hydrogen molecules (and/or atoms), often resulting in ionization. Within circumstellar disks, ionization plays an important role in setting the thermal and chemical properties of the material; for example, the ionization state is crucial for the development of the magneto-rotational instability (MRI), the process that helps drive disk accretion (Balbus & Hawley 1991). On the larger scales of molecular clouds, and their constituent cloud cores, ionization determines, in part, the coupling between the gas (which is mostly neutral) and the magnetic field (Shu 1992).

This paper is organized as follows: In Section 2 we review the stellar initial mass function (IMF), as well as the distributions of cluster masses and other properties. The predicted yields of SLRs are discussed in Section 3, including both the nuclear yields produced by supernovae and the corresponding yields expected per star (obtained by averaging over the stellar IMF). The nuclear yields per cluster are considered next, in Section 4, where we also determine expectation values for the SLR yields per cluster (averaging over the cluster distribution) and the yields expected for an average star in a cluster. The distributions of the SLR abundances delivered to individual solar systems are then constructed in Section 5. Global considerations are discussed in Section 6, including the galaxy-wide star formation rate and molecular cloud inventories of SLRs. Finally, we conclude, in Section 7, with a summary of our results and a discussion of their implications.

2. Stellar and Cluster Mass Distributions

2.1. Initial Mass Function for Stars

The distribution of SLRs will depend on the stellar initial mass function (IMF). This distribution has been studied intensively (see Kroupa 2001; Chabrier 2003 for recent reviews). In its most basic form, the stellar IMF has the form of a log-normal distribution with a power-law tail on the high-mass end and perhaps another tail at the low-mass end (Adams & Fatuzzo 1996). In any case, the distribution is heavily weighted toward stars of low mass (see also Salpeter 1955; Scalo 1998). In this work, however, we are interested in the high-mass end of the stellar IMF, as only stars with mass above the threshold $M_* \gtrsim 8 M_\odot$ contribute to the supply of SLRs through supernova explosions.

For the present application, one useful way to parameterize the stellar IMF is to define $\mathcal{F}_{SN}$ to be the fraction of the (initial) stellar population with masses greater than the minimum mass ($M_* = 8 M_\odot$) required for a star to ends its life with a supernova explosion.

Current observations indicate that $\mathcal{F}_{SN} \approx 0.005$, although this value remains uncertain (e.g., see the models advocated by Adams & Fatuzzo 1996; Kroupa 2001; Chabrier 2003). The mass distribution for massive stars can be written in power-law form

$$\frac{dN_*}{dm} = \mathcal{F}_{SN} \frac{\gamma}{8} \left(\frac{m}{8}\right)^{-(\gamma+1)} , \tag{1}$$

where $m = M_*/(1M_\odot)$ is the mass in Solar units and the canonical value of the index $\gamma \approx 1.35$ (Salpeter 1955). In spite of the large number of studies of the stellar IMF, in many different environments, the power-law form (1) for the high-mass end of the distribution remains robust. However, the value of the index γ appears to have significant scatter from region to region (e.g., Scalo 1998), such that γ is evenly distributed within the range $\gamma = 1.5 \pm 0.5$. For the sake of definiteness, we use $\gamma = 1.5$ as the default value to characterize the high-mass end of the IMF, but allow the index to vary.

As written, the probability distribution of equation (1) is normalized so that

$$\int_8^\infty \frac{dN_*}{dm} dm = \mathcal{F}_{SN} \, . \tag{2}$$

As a result, the distribution is normalized to unity for the entire mass distribution (not just the high mass end), where this statement holds in the absence of a maximum stellar mass. In practice, one expects the stellar IMF to have a maximum stellar mass m_∞, although the value of m_∞ remains uncertain. In order of magnitude, however, both theory and observations suggest that $m_\infty \approx 120$ is a good approximation. If we include this upper mass limit in the integral of equation (2), we obtain a correction factor $[1 - (8/m_\infty)^\gamma] \approx 0.983$ in the normalization. Note that the relative size of this correction factor is much smaller than the uncertainties in the other parameters that specify the IMF. As a result, we ignore this correction for the remainder of this work.

To complete the specification of the stellar IMF we also need the average stellar mass, i.e.,

$$\langle m \rangle \equiv \int \frac{dN_*}{dm} m dm \, . \tag{3}$$

For example, since stellar clusters are often described by their stellar membership size N and/or their mass in stars M, we often need to convert between the two (where $M = N\langle m \rangle$). Similarly, star formation rates can be specified in terms of 'stars per unit time' or 'solar masses per unit time', with the conversion factor $\langle m \rangle$.

To summarize, this paper characterizes the stellar IMF in terms of the three parameters $(\gamma, \mathcal{F}_{SN}, \langle m \rangle)$. Since the stellar IMF is steeply declining for all possible choices of γ, most supernova progenitors have masses in the range $m = 8 - 25$. As a result, the most important

parameter that determines radioactive yields is the fraction of stars $\mathcal{F}_{SN}$ that are above the mass threshold for supernovae.

2.2. Mass Distribution and Properties of Embedded Star Clusters

Stars form within embedded clusters, where the number of members in these systems spans a wide range (e.g., see the reviews of Lada & Lada 2003; Porras et al. 2003; Allen et al. 2007). Unfortunately, current observations are not sufficiently complete to specify the distribution of cluster membership sizes N. Studies of embedded clusters in the Solar neighborhood indicate that the distribution of cluster sizes N is close to a power-law, so that

$$\frac{dN_C}{dN} = \frac{C_N}{N^a}\,, \tag{4}$$

where C_N is a normalization constant and where the index $a \approx 2$. Here, N_C is the number of clusters and N is the number of stellar members in the clusters. Studies that consider more distant clusters also find power-law distributions, again with $a \approx 2$ (e.g., Elmegreen & Efremov 1997; Kroupa & Boily 2003; Whitmore et al. 2007). The simplest possibility is that the cluster distribution has the same power-law form, and the same normalization constant, over the entire range of cluster sizes $N = 1 - 10^6$. For sake of definiteness, we use a single power-law in the present analysis (but one should keep in mind that the power-law distribution observed for small clusters nearby and that observed for large clusters at large distances have not been shown to match up). Further, we adopt a benchmark value of the index $a = 2$. In this case, the constant $C_N \approx 1$.

A related quantitiy is the probability $P_*(N)$ of a star being born within a cluster of membership size N. This probability distribution is obtaining by multiplying dN_C/dN by another factor of N and hence is given by

$$P_*(N) = \frac{C_P}{N}\,, \qquad \text{with} \qquad C_P = \frac{1}{\log[N_{\rm max}]}\,, \tag{5}$$

where we have taken $a = 2$ and assume that clusters range from $N = 1$ to $N = N_{\rm max}$. We expect $N_{\rm max} \approx 10^6$ and hence $C_P \approx 1/(6 \log 10)$. The cummulative probability $\mathcal{P}$ for finding stars in clusters with membership size N or smaller is thus given by

$$\mathcal{P}(N) = C_P \log[N] = \frac{\log[N]}{\log[N_{\rm max}]}\,. \tag{6}$$

As a result, the probability of finding stars in various sized clusters is evenly distributed in a logarthmic sense.

Next we must specify the radial extent of the cluster. To a reasonable degree of approximation, the cluster radius R can be written as a power-law function of the cluster membership size N, i.e.,

$$R = R(N) = R_0 \left(\frac{N}{N_0} \right)^{\alpha} . \tag{7}$$

For the clusters found in the solar neighborhood (Lada & Lada 2003; Porras et al. 2003), equation (7) works well with $R_0 = 1$ pc, $N_0 = 300$, and $\alpha = 1/2$. The cluster sample in the solar neighborhood is limited to the lower end of the cluster membership size distribution – the sample is not large enough to include the largest clusters. If one applies equation (7) to the entire cluster sample (the entire range of N), then the predicted radii are too large for high-mass clusters. We obtain an adequate fit over the entire cluster size range, $10 \leq N \leq N_{\rm max}$, by using index $\alpha = 1/3$.

Finally, we need to specify the spatial distribution of stars within the cluster. For simplicity, we assume that the stars in the cluster follow a simple power-law distribution of density. Numerical (N-body) simulations of early cluster dynamics (Adams et al. 2006) show that this assumption is reasonable and indicates that the power-law index of the density distribution falls in the range $1 \leq p \leq 2$. As a result, the probability distribution for the radial distance (at a given time, including the time of the supernova explosion) is given by

$$\frac{dP}{dr} = \frac{4\pi r^2}{N} n_*(r) = \frac{3-p}{R} \left(\frac{r}{R} \right)^{2-p} , \tag{8}$$

where R is the cluster radius (which varies with cluster membership size N – see equation [7]).

3. Production of Short-lived Radioactive Nuclei

3.1. Synthesis of SLRs in Supernovae

Supernovae produce a wide variety of radioactive nuclei. In this treatment, we consider only the production and distributions of the five most important species of SLRs, namely ^{26}Al, ^{36}Cl, ^{41}Ca, ^{53}Mn, and ^{60}Fe. These species all have half-lives shorter than 10 Myr, and relatively large abundances; these properties, in turn, make them useful for constraining the early history of our Solar System (Cameron 1993; Meyer & Clayton 2000; Ouellette et al. 2007). The abundances of these SLRs are shown as a function of stellar mass in Figures 1 and 2, with the yields taken from the calculations of Woosley & Weaver (1995), Rauscher et al. (2002), and Limongi & Chieffi (2006).

For purposes of finding nuclear enrichment levels for typical solar systems, we often further limit our focus to the two species ^{26}Al and ^{60}Fe, because they provide the largest contribution to the ionization and heating rates. Figure 1 shows the yields for these two SLRs, where we include results from two different sets of stellar nucleosynthesis calculations. The first group (Woosley & Weaver 1995) considers the range of progenitor masses $M_* = 11 - 40 M_\odot$, where these results have been updated (Rauscher et al. 2002) for the more limited range in stellar masses $M_* = 15 - 25 M_\odot$ (see also Timmes et al. 1995a,b; Woosley et al. 2002). For the yields shown in Figure 1, we use the updated yields for the range of masses where they are available; hereafter results from this set of papers are denoted as WW. The second set of results (Limongi & Chieffi 2006), hereafter LC, considers a wider range of masses $M_* = 11 - 120 M_\odot$. As shown in the Figure, the two different sets of nucleosynthesis calculations are not in perfect agreement. Although the predicted yields used here only vary by a factor of ~ 2, and this level of uncertainty is often quoted, we note that even larger variations are possible. The predicted abundances of both ^{26}Al and ^{60}Fe are extremely sensitive to variations in the triple-α reaction (Tur et al. 2010), and the corresponding reaction rates are not precisely known. As a result, the uncertainties in the yields for SLRs can be *larger* than a factor of two. Finally, we note that the yields for the WW models are only given up to $m = 40$. Here we extrapolate to larger values assuming $M_A = constant$ for $m > 40$; although stars more massive than this threshold are rare, this choice provides another source of uncertainty.

For completeness, we show the expected yields of the isotopes ^{36}Cl, ^{41}Ca, and ^{53}Mn in Figure 2 (where these results are taken from the WW group). The abundance of ^{36}Cl is lower than those of ^{26}Al and ^{60}Fe by roughly an order of magnitude, so that its contribution to the ionization rate is correspondingly smaller. On the other hand, while ^{41}Ca and ^{53}Mn have relatively large abundances, they both decay via electron capture, and do not (immediately) emit ionizing energy.

We note that this analysis assumes that all of the SLRs produced by supernova explosions are actually ejected outward and become available for enrichment. In practice, however, calculations of supernovae remain challenging (Mösta et al. 2014), so that the degree of mixing and fallback of synthesized material is not completely known. Indeed, some cosmochemical models suggest some fallback is necessary to explain the particular isotopic abundances observed in the solar system (e.g., Liu 2014). A significant amount of fallback would lower the SLR abundances determined in this paper.

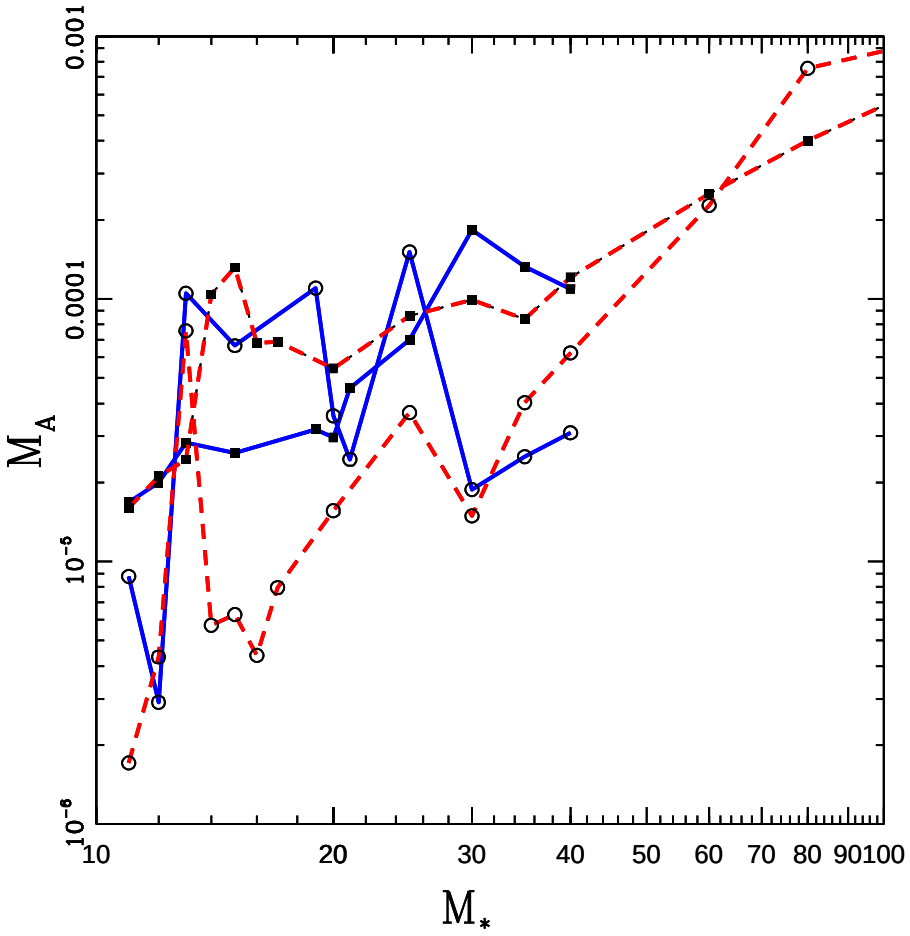


Fig. 1.— Yield M_A of short-lived radioactive nuclei as a function of progenitor mass (both quantities are given in units of $M_\odot$). The curves marked by solid squares indicate the yields for ^{26}Al; the curves marked by open circles indicate yields for ^{60}Fe. Results are presented for two different sets of stellar evolution calculations: Yields from the WW models are shown as blue solid curves (Woosley & Weaver 1995; Rauscher et al. 2002), whereas yields from the LC models are shown as red dashed curves (Limongi & Chieffi 2006).

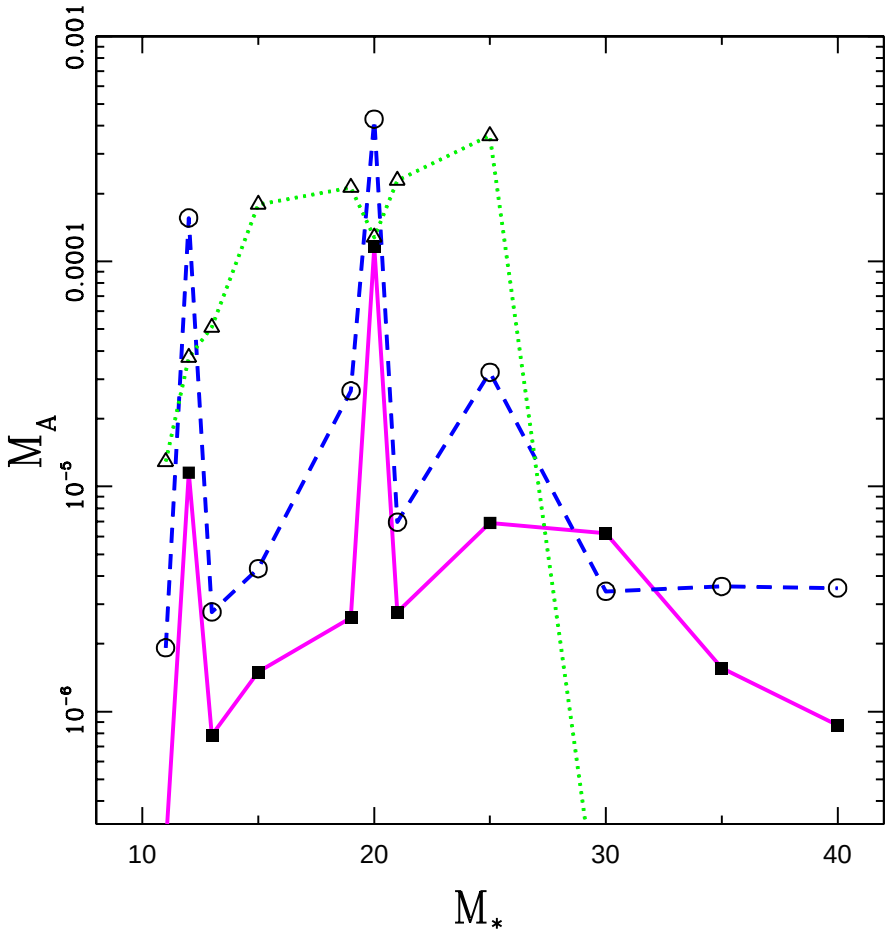


Fig. 2.— Yield M_A of short-lived radioactive nuclei as a function of progenitor star mass (in units of $M_\odot$). Solid magenta curve marked by solid squares indicates the yields for ^{36}Cl; the dashed blue curve marked by open circles provides the yield for ^{41}Ca; the dotted green curve marked by open triangles provides the yields for ^{53}Mn. Results are taken from the WW stellar evolution calculations (Woosley & Weaver 1995; Woosley et al. 2002; Rauscher et al. 2002).

3.2. Nuclear Yields per Star

For a cluster of given membership size N, and for a given stellar IMF, we want to find the abundance distribution for each type of radioactive species (here we denote an arbitrary radionuclide as A_k). As outlined below, we can determine these abundance distributions via sampling. To leading order, however, the distributions can be characterized by their expectation values and widths (or variance). At higher order, however, the distributions show significant departures from gaussians.

To start, we define the yield weighted by the stellar IMF. More specifically, for a given IMF and radionuclide A_k, we define the expectation value per star $\langle M[A_k] \rangle_*$ of the yield to be

$$\langle M[A_k] \rangle_* \equiv \int_{m_{min}}^{m_\infty} M[A_k; m] \frac{dN_\star}{dm} dm \,, \tag{9}$$

where $M[A_k; m]$ is the yield of species A_k for a progenitor star of mass m. The upper limit of integration is set by the maximum stellar mass, which is taken here to be $m_\infty = 120$; since the stellar IMF is a steeply decreasing function of stellar mass, and since the expected yields are not steeply increasing with mass, most of the support for the integral in equation (9) occurs for the smaller masses, so that results are not overly sensitive to the upper limit. The lower limit of integration is set by the minimum mass required for a star to explode and thereby provide nuclear enrichment; this criterion thus implies that $m_{min} \sim 8$. However, the main-sequence lifetime of stars with $m \sim 8$, about 20 Myr, is longer than the expected time for which circumstellar disks retain their gas (3 – 10 Myr; Hernández et al. 2007), and is longer than the lifetime of most embedded clusters (3 – 10 Myr; Allen et al. 2007; Gutermuth et al. 2009). More recent studies based on *Spitzer* observations (Cizea et al. 2007), and SCUBA-2 surveys (Williams et al. 2013), suggest that the lifetime of circumstellar disks could be even shorter, 1 – 3 Myr. As a result, although we use the full range of stellar masses (with $m_{min} = 8$) to compute expectation values, these results can be subject to a reduction factor because of constraints on stellar lifetimes. Finally, we note that the expectation value defined via equation (9) is normalized so that it provides the expected radioactive yield *per star*. Because only the massive stars contribute to the yields, this expectation value per star is much smaller than the radioactive yield per supernova; these yields are smaller by the factor $\mathcal{F}_{SN}$. For the sake of definiteness, we use $\mathcal{F}_{SN} \approx 0.005$ as a standard benchmark value; the nuclear yields can be scaled upward, or downward, for alternate values of $\mathcal{F}_{SN}$.

For the two SLRs of greatest interest, ^{26}Al and ^{60}Fe, Figure 3 presents the expectation value for the yield per star. These yields are plotted here as a function of the index γ of the stellar initial mass function. Note that the yields are given in units of "microsuns" $\mu M_\odot$ (where $1 \mu M_\odot = 10^{-6} M_\odot$). For the WW models of stellar evolution, the nuclear yields vary

slowly with index γ and the values for ^{26}Al and ^{60}Fe are nearly equal (see the blue solid curves in Figure 3). In contrast, for the stellar models of LC, the nuclear yields vary by a factor of ~ 3 over the possible range of the index γ (see the red dashed curves in the Figure). In addition, the yield for ^{26}Al is significantly larger than that for ^{60}Fe. The variations shown in Figure 3 provide a measure of the uncertainty in the yields, due to possible variations in the index of the IMF and/or uncertainties in the stellar nucleosynthesis calculations.

Another source of variation in the nuclear yields arises because the lifetimes of massive stars vary with stellar mass, and these timescales are comparable to the times over which both clusters and disks remain intact. If we consider sufficiently short time scales for disk and cluster evolution, we need to calculate the nuclear yields produced by only those stars with the highest masses. To quantify this effect, Figure 4 presents the nuclear yields per star, calculated using equation (9) with different values for the minimum stellar mass m_{min}. As expected, the yields (per star) decrease steadily with increasing minimum mass. Many previous studies for nuclear enrichment of our Solar System use a progenitor with $m = 25$ as a standard value; a star with this mass spends 6.7 Myr burning hydrogen and a total time of about 7.5 Myr before experiencing core collapse (Woosley et al. 2002). Figure 4 indicates that the yields determined with $m_{min} = 25$ are lower than those obtained with the full spectrum of stellar masses by a factor of ~ 2 (where this factor was obtained by averaging over the four curves shown in the Figure). The ^{26}Al yields from the WW models and the ^{60}Fe yields from the LC models vary by less than this factor, whereas the ^{26}Al yields from the LC models and the ^{60}Fe yields from the WW models vary by a larger factor.

We can also plot the nuclear yields as a function of time, as shown in Figure 5, where only stars that have evolved far enough to explode in time t are included in the yield. This figure is essentially equivalent to Figure 4, where the minimum mass m_{min} is converted into the time required for a star of the given mass to evolve and explode as a supernovae. Stars of the highest mass ($m \sim 100$) have the smallest lifetimes $t \sim 3$ Myr; as a result, the yields are zero for shorter times $t < 3$ Myr. The plot in Figure 5 extends out to about 28.6 Myr, which is the time required for the star with the smallest mass to explode (among those stars that are large enough to end their lives as supernovae). For time scales that exceed this benchmark, all potential supernova progenitors have time to evolve to completion, and the nuclear yields reach their full asymptotic values. Of course, SLRs also decay during such long time intervals (see, e.g., Section 3.3). Although the results vary between the two stellar evolution models (WW and LC), and between the two types of SLRs under consideration (^{26}Al and ^{60}Fe), all of the yields reach about half of their asymptotic values by $t \sim 10$ Myr.

A related quantity of interest is the ratio of the mass in ^{60}Fe produced to that of ^{26}Al. Figure 6 shows this mass ratio as a function of the IMF index γ. Here, the yields of both

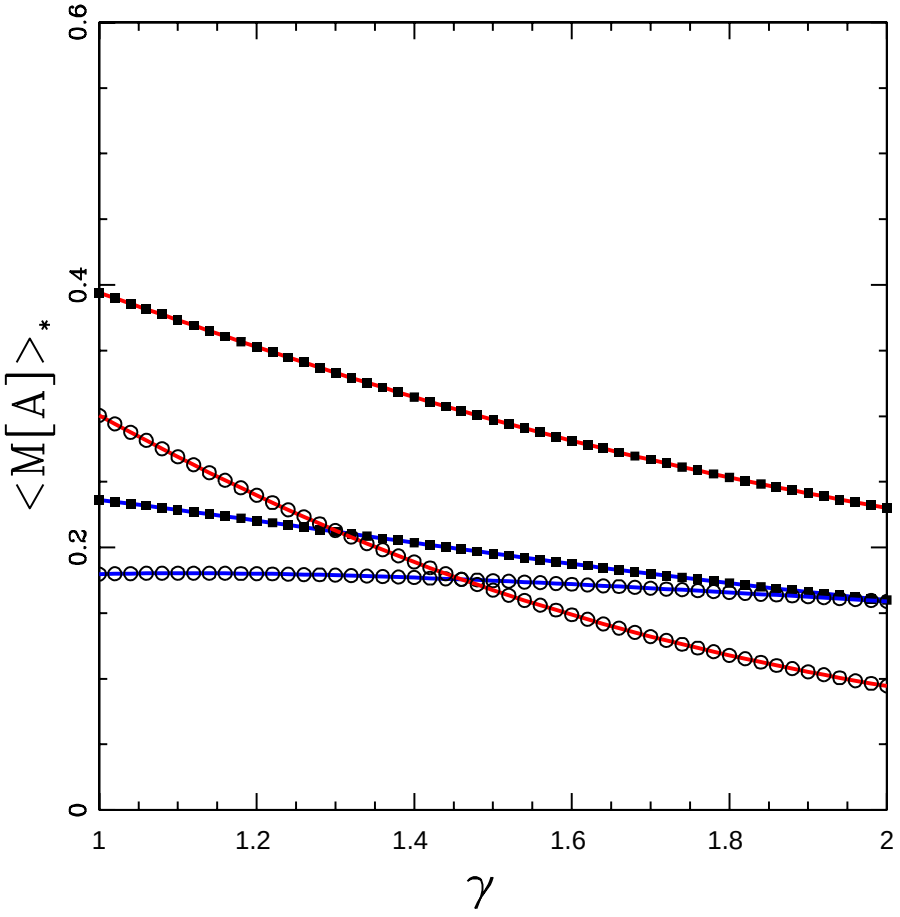


Fig. 3.— Radioactive yields per star for ^{26}Al and ^{60}Fe versus index γ of the stellar IMF. The yields, which are given in units of $\mu M_\odot = 10^{-6} M_\odot$, are proportional to the fraction of stars above the supenova mass threshold, taken here to be $\mathcal{F}_{SN} = 0.005$. Results are shown for the two different sets of stellar evolution calculations, WW (blue solid curves), and LC (red dashed curves). The curves presenting yields for ^{26}Al are marked by solid square symbols, whereas the corresponding curves for ^{60}Fe are marked by open circles.

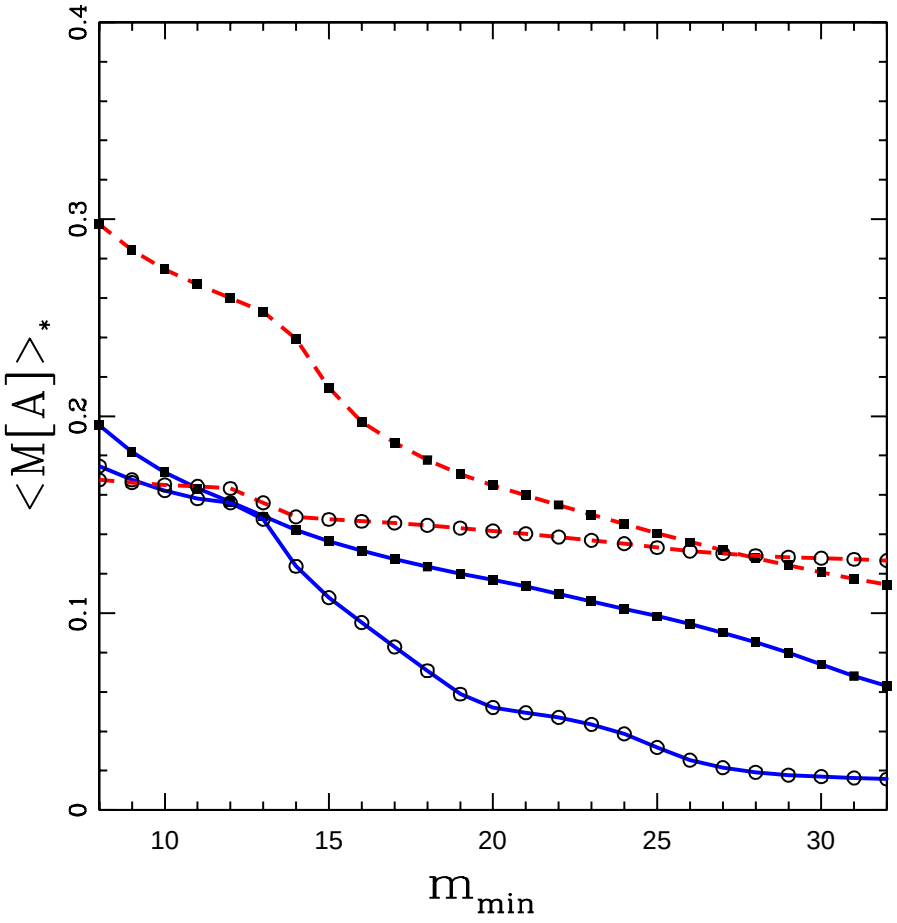


Fig. 4.— Radioactive yields per star for ^{26}Al and ^{60}Fe versus minimum mass of progenitor star included in the distribution. The yields are given in units of $\mu M_\odot = 10^{-6} M_\odot$ and the index of the stellar IMF $\gamma = 1.5$. Results are shown for the two different sets of stellar evolution calculations, WW (blue solid curves), and LC (red dashed curves). The curves presenting yields for ^{26}Al are marked by solid square symbols, whereas the corresponding curves for ^{60}Fe are marked by open circles.

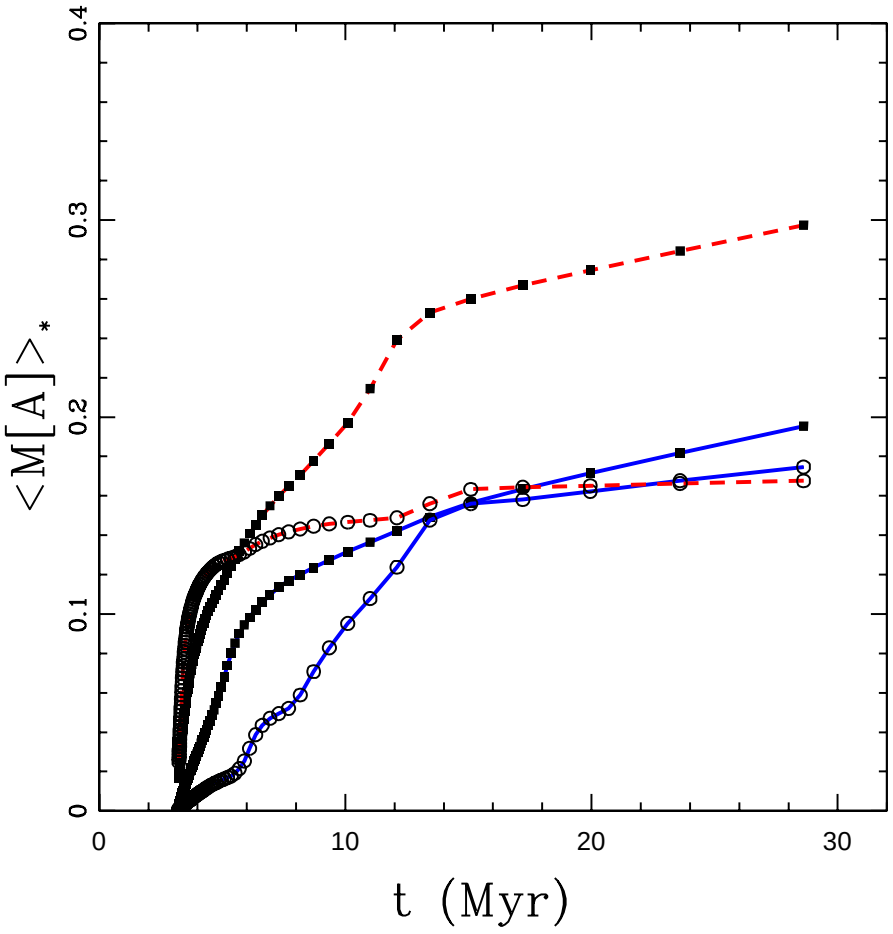


Fig. 5.— Radioactive yields per star for ^{26}Al and ^{60}Fe versus time (in Gyr). For a given time, only those stars that have evolved enough to explode as supernovae are included in the integral over the stellar mass distribution. The yields are given in units of $\mu M_\odot = 10^{-6} M_\odot$ and the index of the stellar IMF $\gamma = 1.5$. Results are shown for the two different sets of stellar evolution calculations, WW (blue solid curves), and LC (red dashed curves). The curves presenting yields for ^{26}Al are marked by solid square symbols, whereas the corresponding curves for ^{60}Fe are marked by open circles.

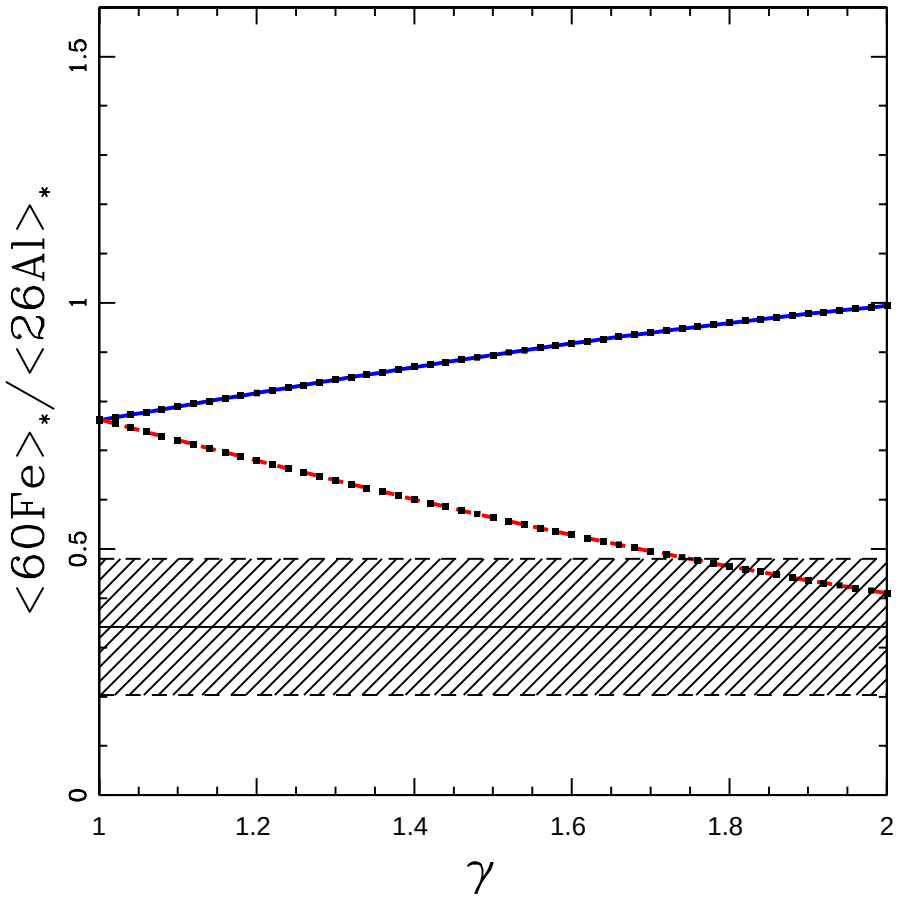


Fig. 6.— Ratio of radioactive yields per star for ^{60}Fe and ^{26}Al, plotted here as a function of the index γ of the stellar IMF (where the yields are given in units of mass). Results are shown for the two sets of stellar evolution calculations, WW (blue solid curve), and LC (red dashed curve). Horizontal line depicts the observed ratio (Diehl et al. 2006; Diehl 2013), where the shaded region delineates the uncertainty in the measurement.

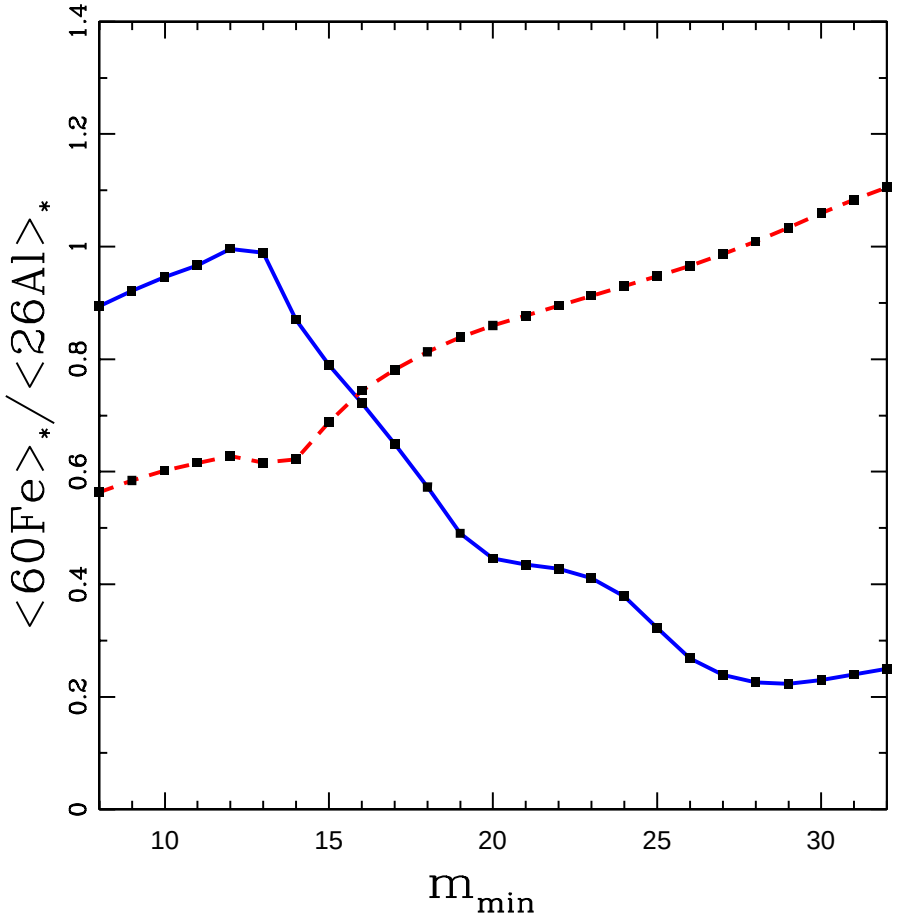


Fig. 7.— Ratio of radioactive yields per star for ^{60}Fe and ^{26}Al, plotted here as a function of the minimum mass of progenitor star included in the distribution. The yields are given in units of mass, and the index of the stellar IMF $\gamma = 1.5$. Results are shown for the two sets of stellar evolution calculations, WW (blue solid curve), and LC (red dashed curve).

nuclear species are averaged over the stellar IMF, and then the mass ratio is found (reversing the order of these operations would produce a different result). This mass ratio also depends on the minimum mass included in the determination of the radioactive yields; the resulting mass ratio is shown as a function of the minimum mass in Figure 7. Whereas the overall yields must decline with increasing minimum mass (Figure 4), the mass ratio displays more complicated behavior. As the index γ increases, the stellar IMF is weighted more toward stars of lower masses; the mass ratio for the WW models increases, whereas the mass ratio for the LC models decreases. Similarly, as the minimum mass increases, the predicted mass ratio decreases for the WW models of stellar evolution, but increases for the LC models.

3.3. Time Evolution

The different species of radioactive nuclei decay at different rates, so their relatative abundances vary with time. Since one important implication of this work is the ionization provided by SLRs, we use the ionization rate to illustate this time dependence. In addition, both molecular clouds and circumstellar disks, the two environments of interest, are composed primarily of H_2, so that we focus on the ionization of molecular Hydrogen. Ionization rates for other species can be scaled accordingly. For a given nuclear species, labeled by the index 'k', the ionization rate ζ_k per hydrogen molecule (Umebayashi & Nakano 2009) is given by the expression

$$\zeta_k = \frac{E_k}{\omega_I} \tau_k^{-1} X_k A_k^{-1} \exp[-t/\tau_k] \,, \tag{10}$$

where E_k is the energy per decay ($\sim$ 1MeV) of the given nucleus, $\tau_k = \tau_{1/2}/\ln 2$ is the decay time, X_k is the mass fraction, and A_k is the atomic weight. The parameter $\omega_I \approx 36$ eV is the average energy required for an energetic particle to produce an electron-ion pair by passing through H_2 gas (Umebayashi & Nakano 2009).

The two most important SLRs are ^{26}Al and ^{60}Fe, which have abundances that are roughly equal when averaged over the stellar IMF (see Figure 3 for further detail). Because of the difference in half-lives, however, ^{26}Al (with $\tau_{1/2} = 0.72$ Myr; Rightmire et al. 1958; Norris et al. 1983) will dominate the ionization rate at early times (measured from the time of the supernova explosion), and ^{60}Fe (with $\tau_{1/2} = 2.6$ Myr; Rugel et al. 2009), will dominate at later times. The third species of possible interest, ^{36}Cl, has a smaller abundance and a shorter half-life ($\tau_{1/2} = 0.3$ Myr; Eckström & Firestone 2004). In addition, the net energy per decay for ^{36}Cl is only about 0.286 MeV, which is appreciably smaller than that of ^{26}Al (3.065 MeV) and ^{60}Fe (2.741 MeV); these values were obtained by averaging the decay energy over the various channels, weighted by the branching ratios, by using the data presented in Table 2 of Umebayashi & Nakano (2009).

The resulting time dependence of the ionization rate is illustrated in Figure 8. Here, we model the averaged expected behavior by considering an effective "supernova" that produces the IMF-averaged yields at $t = 0$. The resulting ionization rate is normalized so that the sum of the contributions from the three SLRs (^{26}Al, ^{36}Cl, and ^{60}Fe) is unity at $t = 0$. The time evolution of the ionization rate then shows the expected behavior: The contribution of ^{36}Cl is minimal and becomes less important with time. Ionization due to ^{26}Al dominates at early times, whereas that due to ^{60}Fe dominates at later times, with the crossover occurring at about $t \approx 3.2$ Myr.

In order to determine the magnitude of the ionization rate, we need to specify the amount of material that is mixed with the supernova ejecta. The radioactive yields (e.g., see Table 1) are given in terms of the mass of SLRs per star (i.e., averaged over the stellar IMF). If we consider the SLRs to be mixed with 1.0 $M_\odot$ of material, for example, the ionization rate per hydrogen molecule would be about $\zeta_0 \approx 5 \times 10^{-17}$ sec^{-1}. This value is comparable to, but somewhat larger than, the ionization rates due to cosmic rays in the interstellar medium (where typical estimates imply $\zeta \approx 1 - 3 \times 10^{-17}$ sec^{-1}; e.g., van der Tak & van Dishoek 2000). Since the star formation efficiency $\epsilon_{\rm sfe}$ is low, the amount of material that the ejecta mix with is expected to be larger by a factor of $1/\epsilon_{\rm sfe} \sim 100$; on the scale of a star-forming region, the ionization rate is thus smaller by this factor, so that we expect $\zeta \sim 10^{-19}$ sec^{-1} (see Section 6). Notice also that one expects a wide range of values for the ionization rates due to both SLRs and cosmic rays (Fatuzzo et al. 2006; Cleeves et al. 2013a,b).

For sufficiently short spans of time, the contribution of SLRs to ionization rates dominates over that of long-lived radioactive species. For the abundance patterns deduced for the Solar Nebula, for example, the contribution from long-lived nuclei is smaller by a factor of $\sim 10^4$ (Umebayashi & Nakano 2009) at the start of the epoch ($t = 0$). For the benchmark case illustrated by Figure 8, the short-lived nuclear species continue to dominate until time $t \approx 16$ Myr. As a result, we ignore the contribution of long-lived nuclei for the remainder of this paper. Nonetheless, this issue should be examined in the future.

4. Distributions of Nuclear Yields for Clusters

4.1. Yields for Clusters in the Large-N Limit

In the limit of large clusters, $N \rightarrow \infty$, the distributions of nuclear yields will approach a gaussian form (see below). For this regime, this section determines the mean values for the distributions and their expected widths, where these quantities are a function of stellar membership size N.

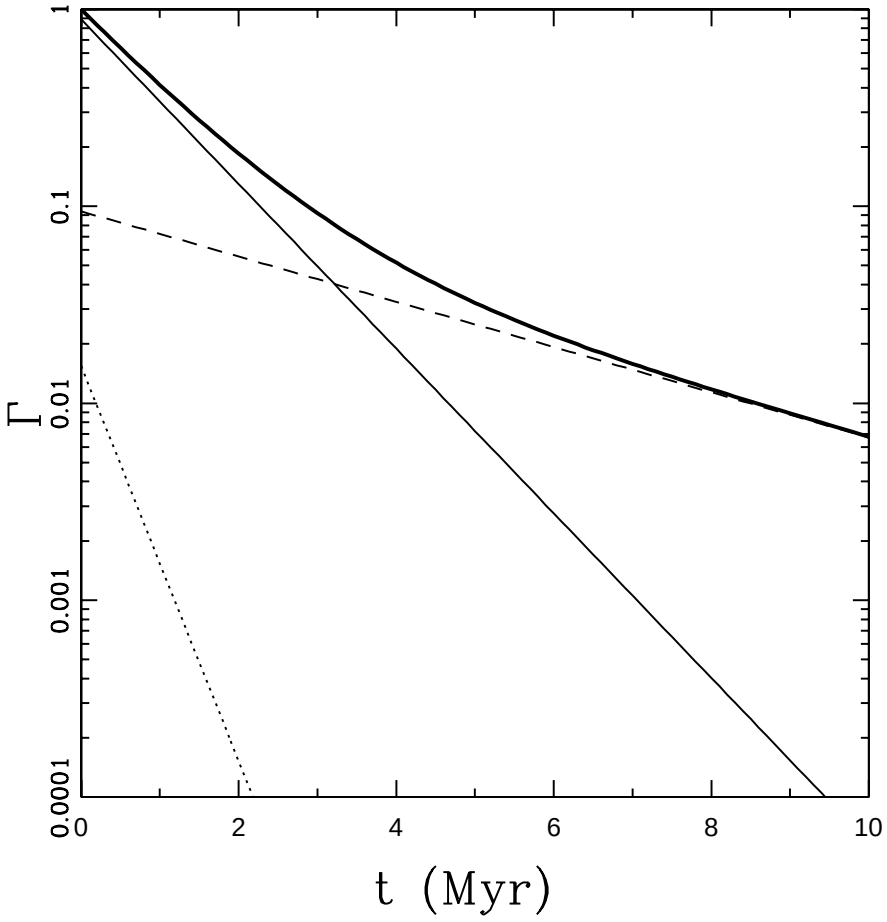


Fig. 8.— Contributions of the three most important nuclear species to the SLR-induced ionization rate (using nuclear yields from the WW stellar evolution models). The ionization rate is normalized to unity at $t = 0$, the time of the supernova explosion. The relative abundances are determined by using the yields per star, which have been averaged over the stellar IMF. The curves correspond to ^{26}Al (solid), ^{36}Cl (dotted), ^{60}Fe (dashed), and the total (heavy solid).

Here, the radioactive yield for a cluster with size N is given by the sum

$$M[A_k; N] = \sum_{j=1}^{N} M[A_k; m_j] \,, \tag{11}$$

where $M[A_k; m_j]$ is the radioactive yield of species A_k from the jth cluster member (with mass m_j). Only the massive stars (with $m_j > 8$) explode as supernovae at the end of their lives and contribute to the radioactive yield of the cluster. As a result, the quantity $M[A_k; m_j] = 0$ for most cluster members.

In this treatment, we assume that the radioactive yield for a given star is determined by the stellar mass, which is drawn independently from a specified stellar IMF. The sum from equation (11) is thus the sum of random variables. Here the variables are the radioactive yields of the individual stars, so that the variables are drawn from a known distribution, which is in turn determined by the IMF and by stellar nucleosynthesis. In the limit $N \gg 1$, the expectation value $\langle M[A_k; N] \rangle$ of the radioactive yield for the cluster is given by

$$\langle M[A_k; N] \rangle = N \langle M[A_k] \rangle_* \,, \tag{12}$$

where $\langle M[A_k] \rangle_*$ is the expectation value of the yield of radioactive species A_k per star, as defined via equation (9). Keep in mind that the radioactive yield for a cluster will converge to the value implied by this expectation value in equation (12) only in the limit of large N. The minimum value of cluster membership N required for this convergence is discussed below. Small clusters often display large departures from the expectation value.

In the limit of large $N \gg 1$, the central limit theorem implies that the distribution of yields $M[A_k; N]$ must approach a gaussian form (e.g., Feller 1968). In practice, however, the convergence is rather slow. In addition, since only a small fraction of stars contribute to the nuclear abundances, large N values are necessary for convergence. One of the issues of interest here is the value of stellar membership N required for statistical considerations to be valid. In the large N limit, where the central limit theorem applies, the resulting gaussian form for the composite distribution is independent of the form of the initial distributions, i.e., it is independent of the stellar IMF and the mass-luminosity relation. The width of the distribution also converges to the value given by

$$\langle \sigma \rangle^2 = \frac{1}{N} \sum_{j=1}^{N} \sigma_j^2 \quad \Rightarrow \quad \langle \sigma \rangle = \sqrt{N} \sigma_* \,, \tag{13}$$

where σ_* is the width of the individual distribution and is defined by

$$\sigma_*^2 \equiv \langle M[A_k]^2 \rangle_* - \langle M[A_k] \rangle_*^2 \,. \tag{14}$$

The expectation values $\langle M[A_k]\rangle_*$ and widths σ_* of the distributions of radioactive yields are listed in Table 1 for the five species of radionuclides considered in this paper (and for our chosen form of the stellar IMF). Results for given for all five isotopes using the WW models of stellar evolution, whereas results are only given for ^{26}Al and ^{60}Fe using the LC models (results are not available for the other nuclear species). Both the expectation values and the widths are given in units of $\mu M_\odot$. For each radioactive species, the expectation value $\langle M[A_k]\rangle_*$ and the width σ_* of the distributions are given for three values of the index γ of the stellar IMF. The results are not overly sensitive to the slope of the IMF in the mass range $m > 8$, primarily because the radioactive yields are not sensitive functions of progenitor mass (see Figures 1 and 2). However, the yields are directly proportional to the fraction $\mathcal{F}_{SN}$ of stars above the supenova mass threshold; for the cases shown in Table 1 we have used $\mathcal{F}_{SN} = 0.005$.

The fifth column in Table 1 lists the number of stars N_X in a cluster required for the width of the distribution for the cluster to be smaller than the expectation value of the yield of the cluster (for the WW yields). Since the expectation value of the yield for a cluster is proportional to N (see equation [12]) and the width of the distribution is proportional to $\sqrt{N}$ (see equation [13]), the benchmark cluster size $N_X = (\sigma_*/\langle M[A_k]\rangle_*)^2$. Notice also that this cluster size N_X is that necessary to make the distribution of yields narrower than its expectation value. Even larger membership sizes N are required for the distribution to approach a pure gaussian form.

Table 1 shows an interesting discrepancy between the results obtained from the two nuclear models. The expectation values for the nuclear yields per star show relatively moderate differences between the WW and LC models (compare columns 3 and 6 for ^{26}Al and ^{60}Fe), as expected from the results shown in Figures 3 – 7. However, the widths of the distributions (compare columns 4 and 7) are much wider for the LC models than for the WW models, especially for ^{60}Fe. Part of this difference arises because the LC models provide results for larger progenitor masses, and the yields increase with mass. The WW models end at $m = 40$, and we use the yields for the $m = 40$ model for all higher masses; an alternate extrapolation scheme could resolve part of this difference. However, the LC models also show a steeper dependence of nuclear yields with progenitor mass, especially for ^{60}Fe (see Figure 1). As shown in the following subsection, the wider distributions for the LC models require larger clusters (in stellar membership size N) to approach gaussian forms for the distribution of radioactive yields per cluster.

Table 1: Parameters for Radio Isotope Distributions

Nuclear Species	γ	$\langle M[A_k]\rangle_{*(WW)}$	$\sigma_{*(WW)}$	N_X	$\langle M[A_k]\rangle_{*(LC)}$	$\sigma_{*(LC)}$
	1.3	0.212	4.18	388	0.333	7.82
^{26}Al	1.5	0.195	3.88	394	0.297	6.92
	1.7	0.180	3.59	398	0.267	6.13
	1.3	0.0142	0.623	1940		
^{36}Cl	1.5	0.0137	0.611	1990		
	1.7	0.0131	0.594	2060		
	1.3	0.0699	2.76	1560		
^{41}Ca	1.5	0.0697	2.74	1540		
	1.7	0.0686	2.70	1550		
	1.3	0.329	7.75	556		
^{53}Mn	1.5	0.326	7.63	549		
	1.7	0.318	7.44	549		
	1.3	0.179	3.52	387	0.213	10.1
^{60}Fe	1.5	0.175	3.48	396	0.168	8.53
	1.7	0.169	3.42	409	0.132	7.16

Table 1: The first column of the table gives the species of radionuclide and the second column lists the index of the stellar IMF. In the third column, $\langle M[A_k]\rangle_*$ is the expectation value of the radioactive yield per star using the WW models, whereas σ_* (fourth column) is the width of the corresponding distribution of yields; both quantities are given in units of $\mu M_\odot = 10^{-6} M_\odot$. In the next column, N_X is the number of stars in a cluster required for the width of the distribution of yields for the cluster to be smaller than the expectation value. For ^{26}Al and ^{60}Fe, the table also lists the expectation value of the yield per star and the corresponding width of the distribution for the LC models.

Table 2: Radio Isotope Properties for the Early Solar Nebula

Nuclide A_k	Daughter D_k	Reference R_k	Half-life $\tau_{1/2}$ (Myr)	Mass Fraction X_k	Mass M_k ($pM_\odot$)	Uncertainty $(\Delta M_k)/M_k$
^{26}Al	^{26}Mg	^{27}Al	0.72	3.8×10^{-9}	190	0.11
^{36}Cl	^{36}Ar	^{35}Cl	0.30	8.8×10^{-10}	44	0.46
^{41}Ca	^{41}K	^{40}Ca	0.10	1.1×10^{-12}	0.055	0.094
^{53}Mn	^{53}Cr	^{55}Mn	3.7	4.0×10^{-10}	20	0.13
^{60}Fe	^{60}Ni	^{56}Fe	2.6	1.1×10^{-9}	55	0.35

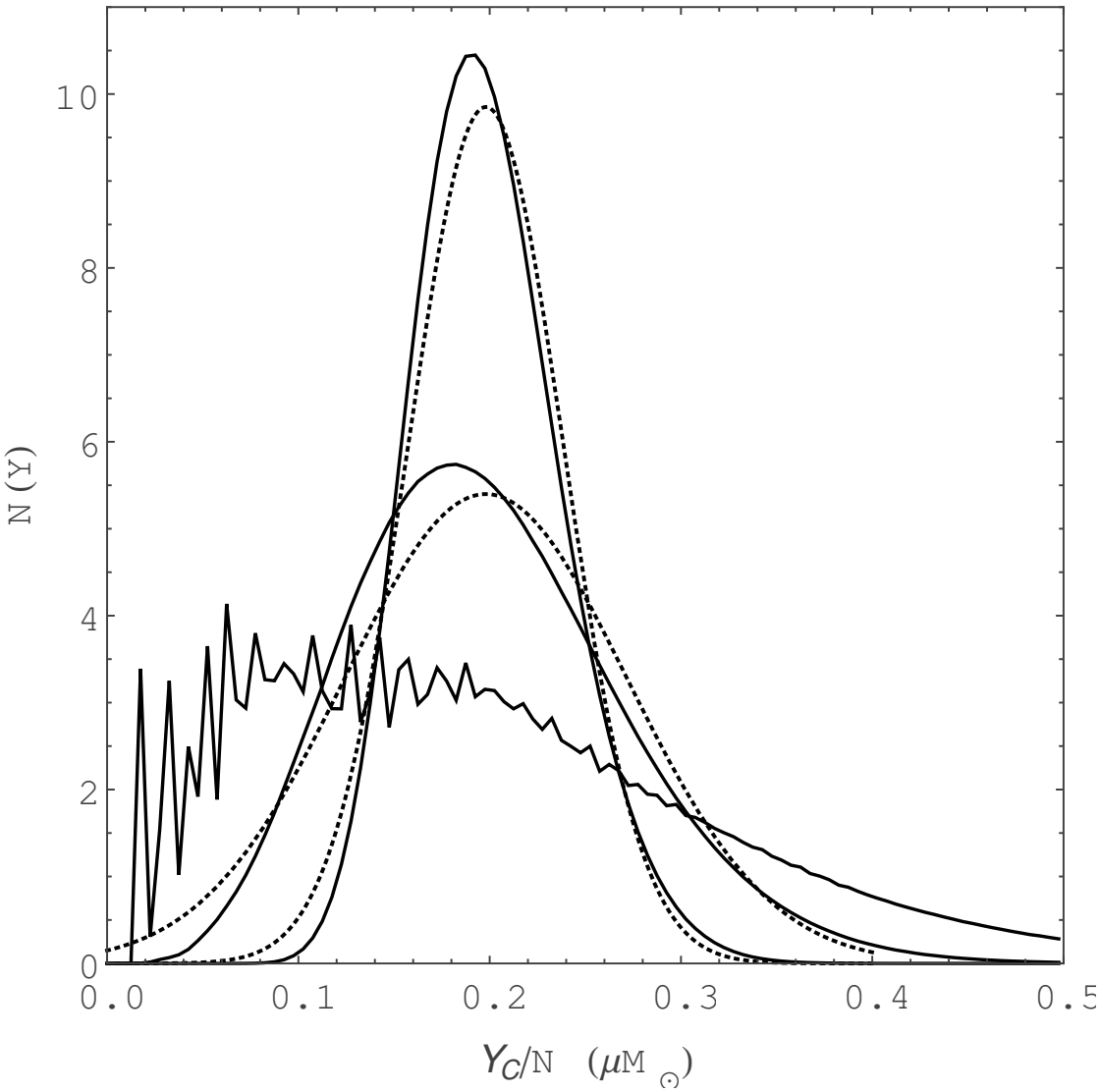


Fig. 9.— Distribution of radioactive yields of ^{26}Al (using WW results) for clusters and $N = 10^4$ (narrow curves), $N = 3000$ (wider curves), and $N = 1000$ (widest, irregular curve). Solid curves show the distributions obtained from sampling the IMF for a large collection of clusters with fixed membership size N. Dotted curves show the corresponding gaussian profile predicted analytically. The yields for all distributions are scaled by the stellar membership size N.

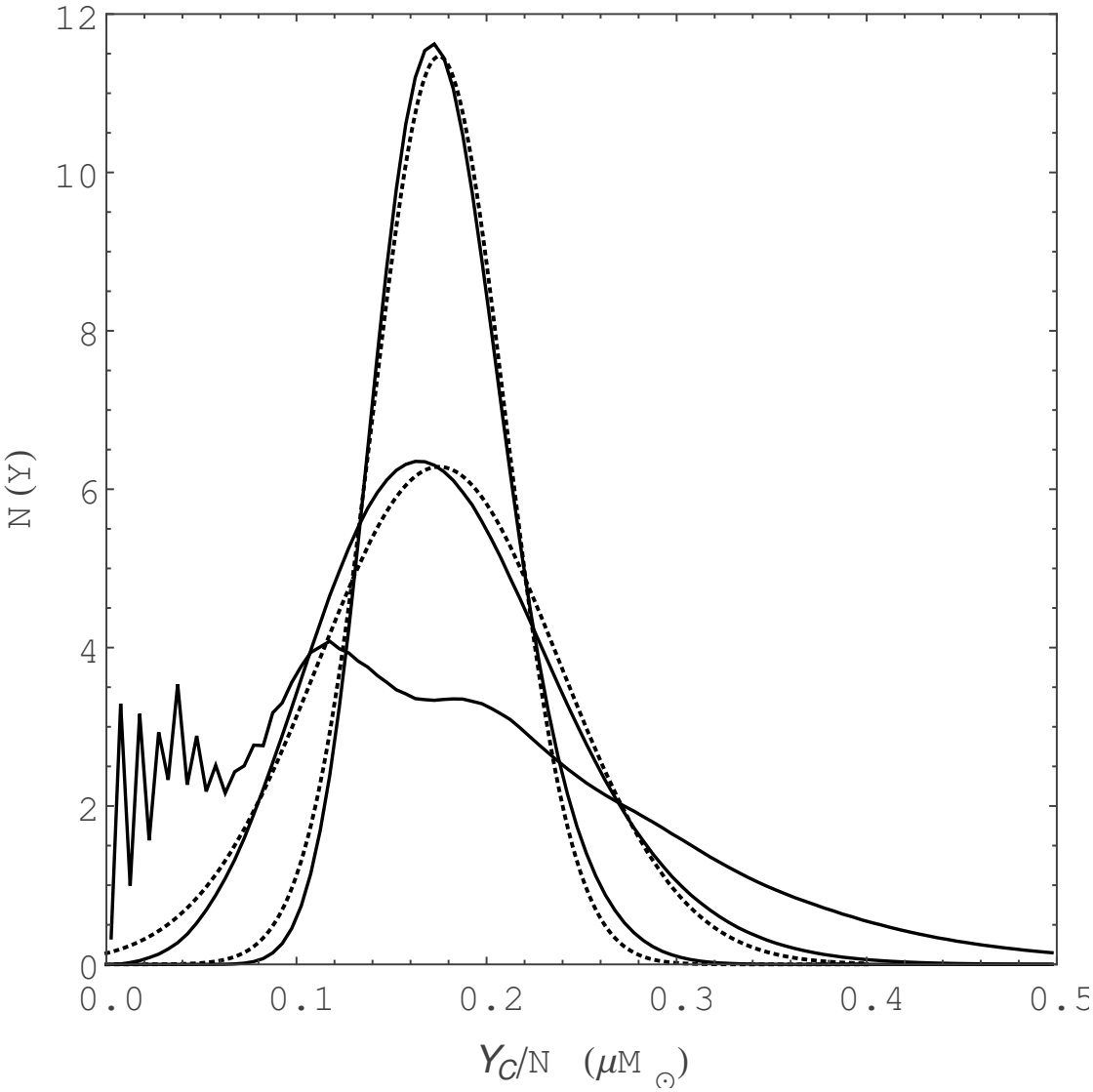


Fig. 10.— Distribution of radioactive yields of ^{60}Fe (using WW results) for clusters and $N = 10^4$ (narrow curves), $N = 3000$ (wider curves), and $N = 1000$ (widest, irregular curve). Solid curves show the distributions obtained from sampling the IMF for a large collection of clusters with fixed membership size N. Dotted curves show the corresponding gaussian profile predicted analytically. The yields for all distributions are scaled by the stellar membership size N.

4.2. Yields for Clusters Determined via Sampling

Next we determine the distributions of nuclear yields for clusters by direct numerical sampling of the stellar IMF. Figure 9 shows the distribution of radioactive yields of ^{26}Al for clusters with fixed stellar membership size $N = 1000$, 3000, and 10^4. The solid curves show the distributions obtained by sampling the IMF for a large number of clusters with fixed N, where the nuclear yields are determined by the WW stellar models. Note that the radioactive yields, shown on the horizontal axis, are scaled by the cluster size N (so that the peak and mean values are nearly independent of N). For comparison, the dotted curves show the gaussian profiles calculated using the mean value from equation (12) and the variance from equation (13). The relative widths of the distributions decrease with increasing N, as expected (see Section 4.1). For the larger stellar membership sizes ($N = 3000$ and 10^4), the clusters contain enough massive stars so that the distributions are close to the gaussian benchmarks. Nonetheless, the true (sampled) distributions are slightly asymmetric, with the peak value somewhat smaller than the expectation value. Although these departures are small for large N, clusters with smaller membership N display large departures from gaussian profiles. The figure also shows the result obtained by sampling clusters with only $N = 1000$ members (shown as the irregular, wide curve). In this case, many clusters only have one or two massive stars large enough to explode, so that the low end of the distribution shows a great deal of structure (which reflects the irregular structure of the radioactive yields as a function of progenitor mass, as shown in Figure 1). Although the spikey nature of the distibution (for $N = 1000$) is visually prominent, perhaps the most important departure from from a gaussian form is the asymmetry toward lower values. As expected, in the opposite limit where $N \to \infty$, the distributions approach true gaussian forms.

Figure 10 shows the corresponding distributions of yields for ^{60}Fe, again using the WW nuclear models and for cluster membership sizes $N = 1000$, 3000, and 10^4. These distributions are analogous to those obtained for ^{26}Al (compare with Figure 9). As expected, the larger clusters (with $N = 3000$ and 10^4) display nearly gaussian profiles, as shown by the dotted curves in the figure. On the other hand, slightly smaller clusters with $N = 1000$ show complicated, irregular structure, for the same reasons discussed above. The distributions are also asymmetric, with the peak value smaller than the mean value; this trend is small for $N \geq 3000$, but significant for $N = 1000$.

Next we consider the effect of the stellar IMF on the resulting distributions of nuclear yields. Figure 11 shows the distributions of yields for clusters with $N = 10^4$ stars and for the WW nuclear models. Results are shown here for both ^{26}Al (red curves) and ^{60}Fe (black curves). For each isotope, distributions for shown for three choices of the index γ of the stellar IMF, where $\gamma = 1.25$ (dashed curves), 1.5 (solid curves), and 1.75 (dotted curves).

The effect of varying the index γ is modest: The distributions shift their mean values slightly as γ varies, as expected given the dependence of the expectation values shown in Figure 3. The expected yields per star decrease with increasingly index γ, so that the distributions move to the left as the stellar IMF becomes steeper. For clusters with different stellar membership sizes N (not shown), one obtains analogous distributions; they are relatively wider for smaller N and narrower for larger N, as illustrated in Figures 9 and 10.

Figure 12 compares the two models for stellar nucleosynthesis used in this work. Here we present distributions of nuclear yields for ^{26}Al and ^{60}Fe, as determined using both the WW and LC results. The cluster membership size is taken to be $N = 10^4$ for this comparison. For the WW models, the distributions are relatively narrow and approach gaussian forms, as depicted by the black curves in the figure (and as shown previously). For the LC models, however, the distributions are markedly wider, as depicted by the red curves. This behavior is in keeping with the larger widths σ_* given in Table 1. For ^{26}Al, the distribution for the LC yields is shifted to the right compared to that for the WW yields — consistent with the larger expectation value found using the LC models — and is close to gaussian. For ^{60}Fe, however, the distribution retains a significantly non-gaussian form, even for this relatively large stellar membership size N. For the LC models, we thus find that larger clusters (larger N) are required for the distributions of nuclear yields to become gaussian, with the effect more pronounced for ^{60}Fe. This behavior results from the steep dependence of the ^{60}Fe yields with progenitor mass (see Figure 1) coupled with the steepness of the stellar IMF: A few, rare large stars can contribute an enormous amount of ^{60}Fe, so that large stellar populations (large N) are required to fully sample the distribution. In this case, the stellar membership size required for a gaussian distribution is larger than $N = 10^4$.

4.3. Expectation Values

In this section we find the expectation values for various quantities of interest. We first consider the expectation value for the radioactive yield Y_C of an entire cluster. To obtain this quantity, we integrate over the distribution of cluster sizes and the distribution of possible radioactive yields (per cluster):

$$\langle Y_C \rangle = \int_1^{N_{max}} \frac{C_N}{N^2} dN \int_0^\infty dY = \int_1^{N_{\rm max}} \frac{C_N}{N^2} dN N \langle M[A_k] \rangle_* = C_N \langle M[A_k] \rangle_* \log N_{\rm max} \,. \quad (15)$$

Since $C_N \approx 1$ and $N_{\rm max} \approx 10^6$, we find that

$$\langle Y_C \rangle \approx 6 \log 10 \langle M[A_k] \rangle_* \,, \quad (16)$$

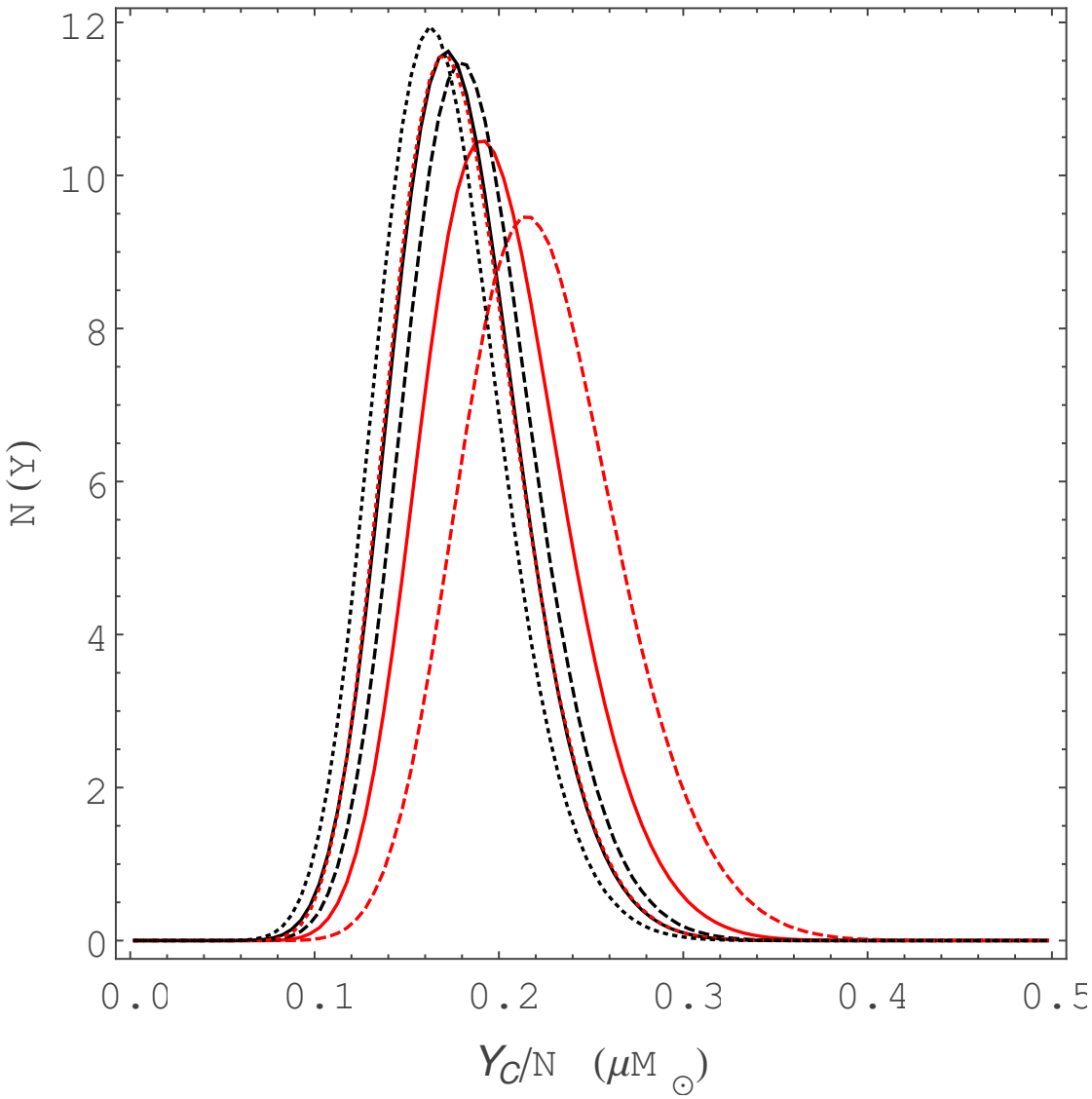


Fig. 11.— Distribution of radioactive yields for difference values of the index γ of the stellar IMF. Distributions are shown for both ^{26}Al (red curves) and ^{60}Fe (black curves) using the WW nuclear model. The cluster size is taken to $N = 10^4$. For each isotope, distributions are shown for three values of the index $\gamma = 1.75$ (dotted curves), 1.5 (solid curves), and 1.25 (dashed curves).

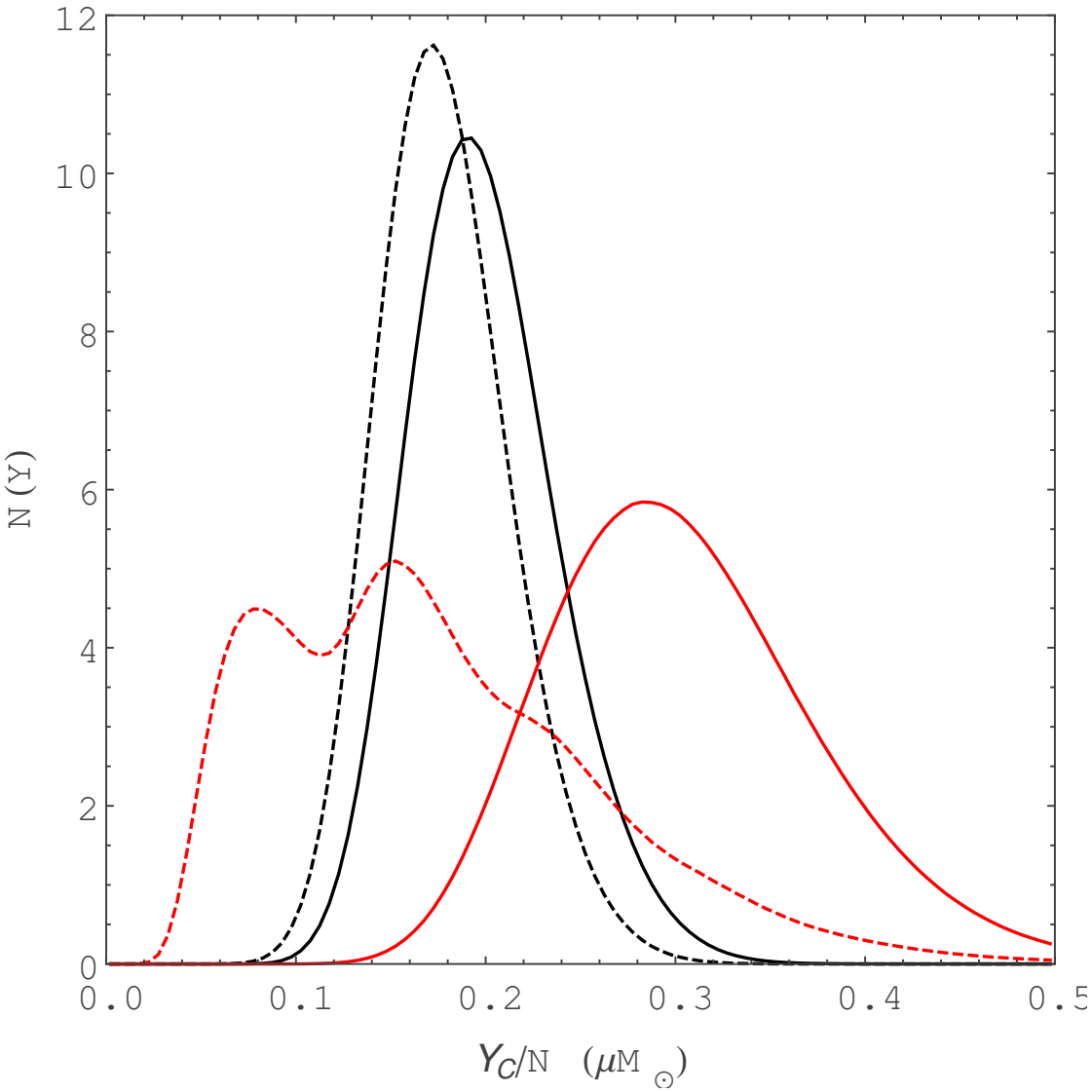


Fig. 12.— Comparison of the two nucleosynthesis models for the distribution of radioactive yields in clusters with $N = 10^4$. The black curves show the distributions for the WW models, whereas the red curves show the distributions for the LC models. The distributions of yields for ^{26}Al are shown as the solid curves, whereas the distributions for ^{60}Fe are shown as dashed curves.

where $\langle M[A_k] \rangle_*$ is the radioactive yield per star for a given nuclear species (as given in Table 1). For example, a "typical" cluster produces only about $2.8 \times 10^{-6} M_\odot$ of ^{26}Al. This value is small because the typical cluster is small: The expectation value for the cluster membership size is given by

$$\langle N \rangle = \int_1^{N_{max}} \frac{C_N}{N^2} N dN = C_N \log N_{\rm max} \approx 14. \tag{17}$$

This expectation value is small because we take the distribution of cluster membership sizes to extend all the way down to $N = 1$. The resulting distribution will thus have many small clusters, which leads to the small value of $\langle N \rangle$. These small clusters contain only a small fraction of the stellar population, however, so that most stars reside in much larger clusters.

A related quantity is the radioactive yield per cluster that a typical star experiences within its birth cluster. This quantity, denoted here as $\langle Y_{C*} \rangle$, is given by

$$\langle Y_{C*} \rangle = \int_1^{N_{max}} \frac{C_P}{N} dN \int_0^\infty dY = \int_1^{N_{\rm max}} \frac{C_P}{N} dN N \langle M[A_k] \rangle_* = C_P \langle M[A_k] \rangle_* N_{\rm max} \, . \tag{18}$$

In this case, $C_P = 1/\log N_{\rm max}$ and we obtain the estimate

$$\langle Y_{C*} \rangle = \frac{N_{\rm max}}{\log N_{\rm max}} \langle M[A_k] \rangle_* \approx 7.2 \times 10^4 \langle M[A_k] \rangle_* \approx 0.0145 M_\odot \, . \tag{19}$$

As considered in the next section, only a small fraction of the nuclear yield from a cluster will be delivered to any given solar system. Before considering that issue in detail, however, it is useful to obtain a rough estimate: If we use a typical distance of a solar system to the cluster center of $d \sim 1$ pc, the expected fraction of the nuclear material that is intercepted by a disk (with radius 30 AU) is only about $f \sim 3 \times 10^{-9}$. If a typical star is born in a cluster with nuclear yield described by equation (19), the expected mass of ^{26}Al impinging on a typical star/disk systems is thus about $4 \times 10^{-11} M_\odot$. For comparison, the estimated mass fraction of ^{26}Al in the early Solar Nebula is $X = 4 \times 10^{-9}$, so that the mass of ^{26}Al is about $2 \times 10^{-10} M_\odot$ (five times larger than the canonical value — see below). Although this argument uses only typical values, it suggests that clusters can provide nuclear enrichment to their constituent solar systems at levels comparable to (but often somewhat less than) those estimated for our Solar Nebula.

5. Distributions of SLR Yields Delivered to Solar Systems

A typical star in a typical cluster will intercept a only fraction f of the radioactive yield produced by the entire cluster. To start, we ignore timing issues. In this limiting case, the

fraction f is given by the geometrical factor

$$f = f(r) = \frac{\pi r_d^2}{4\pi r^2} \cos\theta \,, \tag{20}$$

where r_d is the disk radius, and r is the distance from the solar system to the cluster center (where the high mass stars, and hence the supernova ejecta, originate). The factor of $\cos\theta$ takes into account the fact that the disk is not, in general, facing the supernova blast wave; the distribution of angles is expected to be uniform in $\mu \equiv \cos\theta$ with a mean of 1/2. The radius r must be larger than the radius for which the disk (with disk radius r_d) is stripped due to the blast; for a disk radius $r_d = 30$ AU, and for typical supernova energies, this minimum radial distance $r_{min} \approx 0.1$ pc (Chevalier 2000; Ouellette et al. 2007; Adams 2010).

In this treatment of the problem, we assume that the supernova ejecta are distributed uniformly and isotropically, and are not impeded before reaching the target protoplanetary disks. This scenario is thus idealized, as supernova ejecta can be clumpy (Grefenstette et al. 2014) and intervening molecular cloud material can interfere with nuclear delivery (e.g., see Sashida et al. 2013).

A great deal of previous work has considered the problem of injecting SLRs from supernova ejecta into existing circumstellar disks. The efficiency of injection ranges from essentially 100 percent for injection into circumstellar disks (Looney et al. 2006; Ouellette et al. 2007), down to only about 10 percent for injection into pre-collapse clouds (Vanhala & Boss 2000). For injection into disks, such high efficiencies require the SLRs to condense onto dust grains before striking the disk; more specifically, recent work finds that the efficiencies can be 70 percent or higher only if the grain sizes are larger than $\sim 0.4\mu$m (see Ouellette et al. 2010, in particular their Figure 6). Unfortunately, however, the expected size of grains produced during supernovae remain uncertain. A recent study advocates dust grains with sizes smaller than $\sim 0.1\mu$m (Bianchi & Schneider 2007), which would lead to lower injection efficiencies. In this work, we assume 100 percent efficiency, but the results can be scaled (downward) for any choice of this parameter. Another important issue is the transport of the SLRs after they are acquired; simulations carried out to date suggest that mixing is indeed efficient (Boss 2011, 2013).

5.1. Expectation Values for SLR Delivery

The expectation value $\langle Y_* \rangle$ for the yield of SLRs intercepted by a given solar system takes the form

$$\langle Y_* \rangle = \int_1^{N_{max}} \frac{C_P}{N} dN \int_0^\infty dY \int_{r_{min}}^R \frac{dP}{dr} f(r) dr \,, \tag{21}$$

which can be written

$$\langle Y_* \rangle = \int_1^{N_{\rm max}} \frac{C_P}{N} dN N \langle M[A_k] \rangle_* \int_{r_{min}}^{R} \frac{3-p}{R} \left(\frac{r}{R} \right)^{2-p} \frac{\pi r_d^2}{8 \pi r^2} dr \, , \tag{22}$$

where we have used equation (8) to specifiy the probability distribution of the radial positions and we have taken the mean value of $\cos\theta$. This result can be simplified to the form

$$\langle Y_* \rangle = C_P \langle M[A_k] \rangle_* \frac{(3-p) r_d^2}{8} \int_1^{N_{\rm max}} \frac{dN}{R^{3-p}} \int_{r_{min}}^{R} \frac{dr}{r^p} \, . \tag{23}$$

We can evalute the above result for any value of p and any form for the cluster radius function $R(N)$, which is specified by power-law index α (from equation [7]). For the canonical choices $p = 3/2$ and $\alpha = 1/3$, we obtain

$$\langle Y_* \rangle \approx C_P \langle M[A_k] \rangle_* \frac{3 r_d^2}{4} {r_{min}}^{-1/2} R_0^{-3/2} N_0^{1/2} {N_{\rm max}}^{1/2} \approx 6.3 \times 10^{-5} \langle M[A_k] \rangle_* \, , \tag{24}$$

where we have used typical values to obtain the final approximate equality. Since the yields of both ^{26}Al and ^{60}Fe are of order 0.2 $\mu M_\odot$ (see Figure 3 and Table 1), the typical yield for these SLRs is about 10 – 20 $p M_\odot$ (or $1 - 2 \times 10^{-11} M_\odot$).

The expectation values for SLR yields discussed here are comparable to — but somewhat smaller than — the SLR masses that are inferred for the early Solar Nebula. For comparison, Table 2 lists the isotopes of interest for this paper, along with the daughter products, the reference isotopes, the half-lives, the mass fractions, and the total masses. The abundances listed in the table are inferred from meteoritic data, which has been compiled by numerous previous authors (e.g., see Umebayashi & Nakano 2009; Looney et al. 2006; Young et al. 2005; Dauphas & Chaussidon 2011; and references therein). For each SLR, the total mass is estimated from the mass fraction, where we assume a typical mass for the Solar Nebula of $M_d = 0.05 M_\odot$. We note that the abundance for ^{60}Fe listed here (taken from Tachibana et al. 2006) has been re-measured by other workers (Tang & Dauphas 2012), who found lower abundances. In any case, the total SLR masses listed in Table 2 are somewhat larger than the expectation values discussed above. Taken at face value, this finding implies that Solar System abundances result from the high end of the distribution of possible values. To asssess the probabilties, we need the full distribution, which is determined in the next subsection.

5.2. Distributions for SLR Delivery

Using the probability distributions for cluster yields and for the radial positions of stars within clusters, we can find the distribution of radioactive yields delivered to the constituent

solar systems. Let Y_C be the nuclear yield for a given cluster, where the value of Y_C is distributed according to a probability distribution dP/dY. Let $\xi = r/R$ be the radial position of the recipient solar system within the cluster, where R is the cluster radius; the position is distributed according to $dP/d\xi$, which depends on the density profile of the cluster. The mass M_{ss} of radioactive material delivered to a solar system is given by $M_{ss} = Y_C f(r)$, which can be written as

$$M_{ss} = Y_C \frac{\pi r_d^2}{4\pi R^2 \xi^2} \mu \,, \tag{25}$$

where $\mu = \cos\theta$. To find the distribution of the mass M_{ss} of intercepted nuclear material, we need to specify the distributions dP/dY, $dP/d\xi$, and $dP/d\mu$. The projection factor μ has uniform-random distribution ($dP/d\mu = 1$) on the interval [0,1]. To start, however, we ignore projection effects by setting $\mu = 1$ (projection effects will be reinstated later).

As shown above, for clusters with sufficiently large stellar membership size N, the distribution of yields is nearly gaussian, i.e.,

$$\frac{dP}{dY} = \mathrm{A_Y} \exp\left[-\frac{(Y_C - \langle Y \rangle)^2}{2\sigma^2} \right] , \tag{26}$$

where $\mathrm{A_Y}$ is the normalization constant and is given by

$$\mathrm{A_Y} = \frac{2}{\sqrt{2\pi}\sigma} \left[1 + \mathrm{Erf}\left(\frac{\langle Y \rangle}{\sqrt{2}\,\sigma} \right) \right]^{-1} , \tag{27}$$

where $\mathrm{Erf}(z)$ is the error function (Abramowitz & Stegun 1972). Further, the expectation value $\langle Y \rangle$ and the width σ of the distribution are given by

$$\langle Y \rangle = N \langle Y \rangle_* \qquad \text{and} \qquad \sigma = \sqrt{N}\sigma_* \,, \tag{28}$$

where the quantities with starred subscripts denote the values per star, calculated from convolving the nuclear yields with the stellar IMF.

As discussed earlier, the distribution of radial positions depends on the cluster density profile, i.e.,

$$\frac{dP}{d\xi} = (3-p)\xi^{2-p} \,, \tag{29}$$

where the index p of the cluster density profile lies in the range $1 \le p \le 2$. Note that the radial position has a uniform (constant) distribution for the choice $p = 2$.

Next we define a new variable

$$y \equiv \frac{Y_C}{\langle Y \rangle} \,, \tag{30}$$

so that the mass M_{ss} can be written

$$M_{ss} = \langle Y \rangle \frac{\pi r_d^2}{4\pi R^2} \frac{y}{\xi^2} = M_0 X \, , \tag{31}$$

where the second equality defines the composite variable

$$X \equiv \frac{y}{\xi^2} \, , \tag{32}$$

and the benchmark scale

$$M_0 \equiv \langle Y \rangle \frac{\pi r_d^2}{4\pi R^2} \, . \tag{33}$$

For typical values we obtain

$$M_0 = 0.84 p M_\odot \left(\frac{N}{3000} \right) \left(\frac{\langle Y \rangle_*}{0.2 \mu M_\odot} \right) \left(\frac{r_d}{30 \, \mathrm{AU}} \right)^2 \left(\frac{R}{2 \, \mathrm{pc}} \right)^{-2} \, . \tag{34}$$

The benchmark mass scale is thus of order $1 p M_\odot = 10^{-12} M_\odot$; further, cluster radii are observed to vary as $R \propto N^\alpha$, where $1/4 \leq \alpha \leq 1/2$, so that this mass scale is a slowly varying function of stellar membership size N. For comparison, the inferred abundances of SLRs for the early Solar Nebula correspond to masses in the range 20 – 200 $p M_\odot$ (Table 2). Note that the expected value for the enrichment mass is given by the expectation value $M_0 \langle X \rangle$, which will be larger than M_0. We can evalulate the quantity $\langle X \rangle$ to obtain

$$\langle X \rangle = \int_0^\infty X \frac{dP}{dX} dX = \frac{(3-p)}{(p-1)} \left[\frac{\xi_{min}^{-(p-1)} - 1}{1 - \xi_{min}^{3-p}} \right] \left[1 + B \lambda^2 \exp(-1/2\lambda^2) \right] \, , \tag{35}$$

where the constants B and λ are defined below. We also have introduced a minimum radius $\xi_{min} = r_{min}/R$ for the solar system location within the cluster, and adjusted the normalization constant accordingly. Without this cutoff, the solar system could lie arbitrarily close to the enrichment sources and the integral would diverge. In practice, solar systems that are too close to the cluster center, where the supernova explosions occur, will have their disks destroyed; as a result, blast wave physics enforces a minimum radius of $0.1 - 0.2$ pc (Chevalier 2000; Ouellette et al. 2007; Adams 2010), which implies $\xi_{min} \sim 0.05 - 0.20$. Under most circumstances, $\lambda \ll 1$ and $\xi_{min} \ll 1$; in this limit, the expectation value reduces to the simpler form

$$\langle X \rangle \to \frac{(3-p)}{(p-1)} \frac{1}{\xi_{min}^{p-1}} \, . \tag{36}$$

This expectation value thus has a typical value $\langle X \rangle \sim 10$. The corresponding expected value for radioactive mass enrichment is thus about 10 $p M_\odot$, roughly comparable to, but still somewhat smaller than, the levels inferred for the early Solar Nebula.

The distribution for the scaled variable y takes the form

$$\frac{dP}{dy} = \mathrm{A_Y}\langle Y\rangle \exp\left[-\frac{\langle Y\rangle^2}{2\sigma^2}(y-1)^2\right], \tag{37}$$

where the normalization constant $\mathrm{A_Y}$ is given by equation (27). If we define the quantity

$$\lambda \equiv \frac{\sigma}{\langle Y\rangle} = \frac{\sigma_*}{\sqrt{N}\langle M[A_k]\rangle_*}, \tag{38}$$

the distribution simplies to the form

$$\frac{dP}{dy} = B\exp\left[-\frac{(y-1)^2}{2\lambda^2}\right], \tag{39}$$

where the normalization constant is given by

$$B = \frac{2}{\sqrt{2\pi}\lambda}\left[1+\mathrm{Erf}\left(\frac{1}{\sqrt{2}\,\lambda}\right)\right]^{-1}. \tag{40}$$

Now we need to determine the cummulative probability $P(X)$ for the variable X. The probability is given by the double integral

$$P(X) = \int_0^1 d\xi \frac{dP}{d\xi}\int_0^{X\xi^2}\frac{dP}{dy}dy\,, \tag{41}$$

which can be written in the form

$$P(X) = \int_0^1 d\xi(3-p)\xi^{2-p}\int_0^{X\xi^2} dy\, B\,\exp\left[-\frac{(y-1)^2}{2\lambda^2}\right]. \tag{42}$$

The differential probability is then given by

$$\frac{dP}{dX} = (3-p)B\int_0^1 d\xi\,\xi^{4-p}\exp\left[-\frac{(X\xi^2-1)^2}{2\lambda^2}\right]. \tag{43}$$

For large $X \gg 1$, this result reduces to the power-law form

$$\frac{dP}{dX} \approx \frac{(3-p)}{1+\mathrm{Erf}\left[\sqrt{2}/(2\lambda)\right]}X^{-(5-p)/2}\frac{1}{\lambda\sqrt{2\pi}}\int_0^\infty u^a du \mathrm{e}^{-(u-1)^2/2\lambda^2} \equiv CX^{-(5-p)/2}, \tag{44}$$

where the second equality defines the normalization constant C and where we have defined $a = (3-p)/2$. In the limit where $\lambda \ll 1$, the expression simplifies to the form

$$\frac{dP}{dX} = CX^{-(5-p)/2} \qquad \text{where} \qquad C = \frac{1}{2}(3-p)\,. \tag{45}$$

One quantity of interest is the fraction of solar systems that will be enriched in SLRs above a given threshold specified by X_*. Note that the mass of SLRs is given by $M = M_0 X$, where the benchmark mass is of order $1pM_\odot$. The fraction of systems that receive $X > X_*$ ($M > M_*$) can be written in the form

$$P(X > X_*) = \frac{C}{(3-p)/2} X_*^{-(3-p)/2} \approx X_*^{-(3-p)/2} \,. \tag{46}$$

The treatment thus far has neglected projection effects. Since circumstellar disks are not, in general, aligned toward the supernova ejecta, the distribution derived above must be convolved with the distribution of orientation angles. In practice, we have the probability distribution dP/dX for the variable X that specifies the SLR masses delivered to individual solar systems (where $M = M_0 X$). We need to find the corresponding probability distribution dP/dZ for the composite variable $Z \equiv \mu X$, where $\mu = \cos\theta$ is distributed uniformly on [0,1]. The cummulative probability is then given by the integral

$$P(Z > Z_*) = \int_0^1 d\mu \int_{Z_*/\mu}^\infty \frac{dP}{dX} dX \,. \tag{47}$$

Since we are interested in the regime where $X, Z \gg 1$, we can use the limiting form given by equation (45) to specify dP/dX; as a result, the expression becomes

$$P(Z > Z_*) = \int_0^1 d\mu \int_{Z_*/\mu}^\infty C X^{-(5-p)/2} dX \,, \tag{48}$$

which can be evaluated to obtain

$$P(Z > Z_*) = \frac{2}{5-p} Z_*^{-(3-p)/2} \,. \tag{49}$$

As a result, the fraction of solar systems that are enriched at a given level is reduced by a factor of $2/(5-p) \approx 0.5 - 0.67$ due to projection effects. The corresponding differential probability for the variable Z then becomes

$$\frac{dP}{dZ} = \frac{3-p}{5-p} Z^{-(5-p)/2} \,. \tag{50}$$

To fix ideas, we use the index $p = 3/2$ and require that $Z = \mu X > 100$, which corresponds to nuclear enrichment at levels comparable to those inferred for the early Solar Nebula. Using equation (49), the fraction of solar systems that are enriched at this level is found to be $P(Z > 100) \approx 0.018$. For the extreme values $p = 1$ (2), we obtain $P(Z > 100) = 0.005$ (0.067). This result suggests that only a few percent of all circumstellar disks are enriched at levels comparable to our Solar System (similar results are advocated by Parker et al.

2014). However, for somewhat lower enrichment levels (say, $Z > 10$), the fraction increases to ~ 10 percent for clusters with $p = 3/2$ and to ~ 21 percent for clusters with $p = 2$. For comparison, after taking into account the projection factor, the expectation value is about $\langle Z \rangle \sim 5$ (see equations [31 – 36]). Note that this expectation value is larger than the median because the distribution has a long tail corresponding to high values of enrichment.

This semi-analytic treatment works well for sufficiently large clusters. For example, Figure 13 shows the distribution of the total mass in ^{26}Al that is delivered to constituent solar systems in clusters with membership size $N = 3000$. The solid curve shows the distribution obtained from numerical sampling, whereas the dashed curve shows the result obtained from equations (43) and (33). To obtain the numerical curve, we construct a theoretical sample of one million clusters with $N = 3000$. For each cluster, the stellar IMF is sampled $N = 3000$ times; for the massive stars, the yield of ^{26}Al is then determined using the WW models. With the total supply of ^{26}Al specified for the cluster, the amount delivered to individual solar systems is determined from equation (25) after sampling the distribution of radial positions, as given by equation (8). For both distributions, the cluster radius is given by equation (7) and the index of the cluster density distribution is $p = 3/2$. The semi-analytical result is in excellent agreement with the numerically determined distribution, provided that the same parameters are used.

The distributions shown in Figure 13 are subject to additional uncertainties. For example, we have used the cluster radius from equation (7), which implies $R \approx 3.16$ pc. Some clusters could have slightly smaller radii (say, $R \sim 2$ pc), which would increase the SLR masses by a factor of $\sim 5/2$. In addition, the yields of SLR from the stellar evolution models are uncertain (see Figures 1, 3, 4, and 5). Fortunately, however, the semi-analytic treatment allows us to scale the whole distribution for any choice of supernova yields — one just needs to scale the benchmark mass scale M_0 given by equation (33) for the preferred choice of expectation value, as well as specify the width of the distribution λ using equation (38). Similarly, we can find the distributions for other SLR species (e.g., ^{60}Fe) by using the appropriate values of M_0 and λ. Finally we note that the SLR abundances quoted here do not include radioactive decay, so they represent the starting abundances, immediately after injection. The subsequent decay results in a reduction factor, e.g., as shown in Figure 8 as a function of time since the supernova explosion (see also Section 3.3 and the discussion of Section 7).

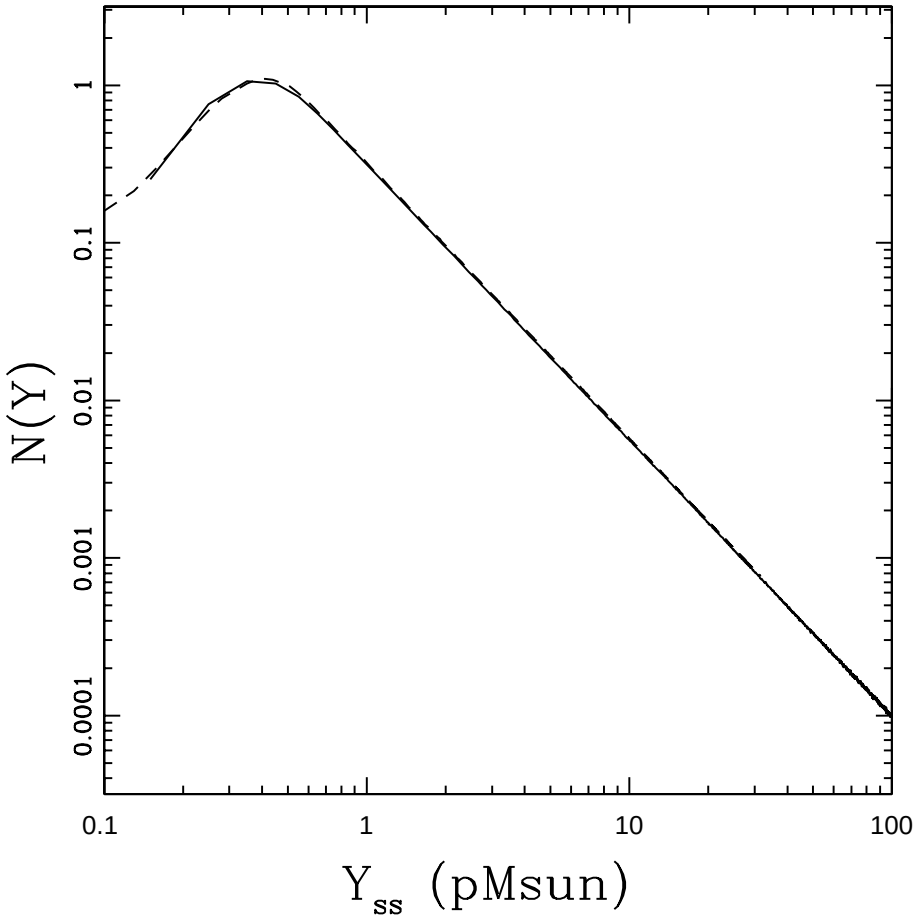


Fig. 13.— Distribution of total mass in ^{26}Al delivered to solar systems living in clusters with stellar membership size $N = 3000$. Solid curve shows the composite distribution calculated by numerical sampling both the stellar IMF and the radial positions within the cluster (using density profile with index $p = 3/2$). The dashed curve shows the analytic distribution given by equation (43) with benchmark mass scale given by equation (33).

6. Global Considerations

The radioactive yields considered here produce observable consquences on larger scales. We note that production of SLRs has been considered previously on galactic scales (e.g., Timmes et al. 1995a,b; Diehl et al. 2006) and in molecular clouds (e.g., Gounelle & Meibom 2008). This section briefly revisits the issue to see how observations on these larger scales can constrain the distributions of SLR enrichment considered in previous sections.

Let Γ_{SF} be the star formation rate of a well-defined system. Here we consider the "system" to be either the entire Galaxy or, on a smaller scale, a molecular cloud complex. For a given system, the time evolution of the supply of radioactive elements, of species A_k, is given by

$$\frac{dM[A_k]}{dt} = \frac{1}{\langle m \rangle} \Gamma_{SF} \langle M[A_k] \rangle_* - \frac{\ln 2}{\tau_{1/2}} M[A_k] \,, \tag{51}$$

where $\tau_{1/2}$ is the half-life; note that the star formation rate is given in units of mass per unit time (rather than the number of stars per unit time). The steady-state condition, which sets the equilibrium abundance, can then be written in the form

$$M[A_k] = \frac{\tau_{1/2} \Gamma_{SF} \langle M[A_k] \rangle_*}{(\ln 2) \langle m \rangle} \,. \tag{52}$$

This simple treatment assumes that the radioactive nuclei decay, but cannot leave the system by other channels. Since the half-lives of interest are short, of order 1 Myr, this assumption should be valid for the Galaxy as a whole. For molecular clouds, however, supernovae may not inject all of their SLRs into the cloud, so that losses can occur.

6.1. Galactic Nuclear Abundances

For the Milky Way galaxy, the current star formation rate is estimated to be $\Gamma_{SF} \approx 1.9 \pm 0.40\ M_\odot\ \mathrm{yr}^{-1}$, where this result (and error estimate) takes into account many independent lines of evidence (Chomiuk & Povich 2011). By definition, the corresponding supernova rate Γ_{SN} is then given by

$$\Gamma_{SN} = \frac{\mathcal{F}_{SN}}{\langle m \rangle} \Gamma_{SF} \,. \tag{53}$$

For our nominal values $\langle m \rangle = 0.5$ and $\mathcal{F}_{SN} = 0.005$, we thus obtain a supernova rate of 0.019 explosions per year, or, one supernova every 53 years.

Using the star formation rate discussed above (Chomiuk & Povich 2011), or the corresponding supernova rate (equation [53]), we can estimate the abundances of the nuclear

species of interest for the Galaxy. The equilibrium abundance of ^{26}Al is given by $M[^{26}\mathrm{Al}] = 0.78\ M_\odot$ ($1.20\ M_\odot$) for the WW (LC) stellar evolution calculations, where we haved used $\gamma = 1.5$ as the index of the stellar IMF. Similarly, for ^{60}Fe abundances, we obtain $M[^{60}\mathrm{Fe}] = 2.77\ M_\odot$ ($2.64\ M_\odot$) for the WW (LC) models. The ^{60}Fe abundances are nearly the same for the two models, whereas the LC model predicts $\sim 50\%$ more ^{26}Al; these results are a direct reflection of the yields shown in Figure 3.

Observations of gamma ray emission, in particular the 1808.65 keV line from ^{26}Al, indicate that the current abundance of ^{26}Al in the Galaxy is $2.8 \pm 0.8\ M_\odot$ (Diehl et al. 2006). This value is larger than the estimate found above by a factor of ~ 2.3 (where we use results from the newer LC models). Observations of the corresponding lines from ^{60}Fe indicate that the line ratio of ^{60}Fe to ^{26}Al is $R(\mathrm{Fe/Al}) = 0.148 \pm 0.06$ (Wang et al. 2007). In steady state, the ratio of line strengths is proportional to the ratio of yields expressed in terms of number of nuclei; we thus have to correct the mass ratio of the yields of ^{60}Fe to ^{26}Al by the ratio 26/60 of their atomic weights. For IMF index $\gamma = 1.5$, the ratio of ^{60}Fe to ^{26}Al by mass is 0.67 (using LC models) so that the predicted line ratio becomes $R(\mathrm{Fe/Al}) = 0.29$, larger than the observed line ratio by a factor of about two. A similar conclusion was reached by Prantzos (2004); the line ratio obtained in that work depends on the maximum stellar mass included in the analysis, as well as the possible contribution from Wolf-Rayet stars.

Given the masses of ^{26}Al and ^{60}Fe inferred for the Galaxy, we can divide by the total mass in gas (about $10^{10} M_\odot$, e.g., Stahler & Palla 2004) and thereby obtain Galaxy-averaged abundances. The resulting mass fractions are $X_{\mathrm{Al}} \sim 3 \times 10^{-10}$ and $X_{\mathrm{Fe}} \sim 10^{-10}$. As expected, these mass fractions are smaller than those inferred for the early Solar Nebula by an order of magnitude for both ^{26}Al and ^{60}Fe (hence the need for radioactive enrichment).

To summarize: We find that the predicted values for both the overall production rate of ^{26}Al and the ratio of ^{60}Fe to ^{26}Al agree with observations at the factor of two level. This apparent discrepancy can be interpreted in two ways: We can use this level of agreement as an estimate for the uncertainties inherent in the results of the rest of this work (the calculated distributions of nuclear yields, etc.), i.e., our results would be uncertain by a factor of two. On the other hand, both the overall abundances and the line ratio can be understood (to higher precision) if twice as much ^{26}Al is produced while keeping the production rate of ^{60}Fe the same.

Possible uncertainties in the theoretical formulation that affect this discrepancy include the following:

[1] The yield of ^{26}Al calculated here assumes a value of $\mathcal{F}_{SN} = 0.005$. The IMF for

high-mass stars could have a larger percentage of high mass stars (larger $\mathcal{F}_{SN}$). However, increasing $\mathcal{F}_{SN}$ would increase the yields of both ^{26}Al and ^{60}Fe by the same factor, so that the line ratio would still be in disagreement.

[2] We have assumed that the index of the IMF $\gamma = 1.5$. Smaller values of the index result in more high-mass stars in the tail of the distribution and hence larger yields (see Figure 3). However, smaller values of γ increase the ratio of ^{60}Fe to ^{26}Al, which works in the wrong direction (see Figure 6). If, instead, we increase the value of the index to $\gamma = 2$, the mass ratio decreases to 0.46, which implies a corresponding line ratio $R(\mathrm{Fe/Al}) = 0.20$. This value is consistent (within the error bars) with the observed value of $R(\mathrm{Fe/Al}) = 0.148 \pm 0.06$. However, this correction would make the overall abundance levels smaller (see Figure 3), requiring another adjustment (e.g., larger $\mathcal{F}_{SN}$) to produce the correct overall yields.

[3] The star formation rate for the Galaxy could be underestimated. However, the estimate used here includes multiple constraints (see Chomiuk & Povich 2011), so that changing the star formation rate could result in disagreement with other observations. In addition, a larger star formation rate would increase the abundance of ^{26}Al, but would leave the line ratio unexplained.

[4] The radioactive yields per star, as determined from the stellar evolution models, could require modification. Yields from the current stellar models most likely contain uncertainties at (approximately) the factor of two level, as indicated by the differences between the models.

[5] The galaxy could have an additional source of ^{26}Al. In this scenario, supernovae would provide all of the ^{60}Fe and half of the ^{26}Al, thereby allowing the star formation rate and stellar IMF parameters to have their canonical values. In this case, the other half must come from other sources, which could include winds from massive stars (Prantzos 2004), Type Ia supernovae (from white dwarfs), and spallation sources (including X-winds; see Shu et al. 2001; Gounelle et al. 2006). The presence of spallation sources are indicated for our own Solar System by evidence for short-lived ^{10}Be (McKeegan et al. 2000), because this SLR cannot be produced via stellar nucleosynthesis. Spallation from X-winds can also produce the isotopes ^{36}Cl, ^{53}Mn, and ^{41}Ca at the levels inferred for the early Solar nebula, but ^{26}Al is underproduced by factors of a few (Shu et al. 2001; see also Chaussidon & Gounelle 2006; Desch et al. 2010 for additional discussion).

6.2. Molecular Cloud Nuclear Abundances

Next we find the equilibrium abundances of the SLRs on the smaller scale of molecular clouds using equation (52). In this setting, the star formation rate Γ_{SF} is that of the cloud.

Star formation is notoriously inefficient (Shu et al. 1987; McKee & Ostriker 2007), where only a small fraction $\epsilon_{\rm sfe}$ of the mass of the cloud is turned into stars during a free-fall time $\tau_{\rm ff}$. As a result, the star formation rate can be written in the form

$$\Gamma_{SF} = \epsilon_{\rm sfe} \frac{M_{\rm cloud}}{\tau_{\rm ff}} \,, \tag{54}$$

where $M_{\rm cloud}$ is the mass of the entire cloud. The free-fall time $\tau_{\rm ff}$ takes the form

$$\tau_{\rm ff} = \left(\frac{3\pi}{32 G \rho} \right)^{1/2} \,. \tag{55}$$

The appropriate mass density ρ is that corresponding to number density $n \approx 10^3$ cm^{-3}, so that the free-fall time $\tau_{\rm ff} \approx 1.2$ Myr. If we adopt this value for $\tau_{\rm ff}$, then equation (54) is exact if we use it as the definition of the star formation efficiency $\epsilon_{\rm sfe}$. The equilibrium mass fraction of a given SLR can be determined by combining equations (52) and (54), i.e.,

$$X_k = \frac{\epsilon_{\rm sfe}}{\ln 2} \frac{\tau_{1/2}}{\tau_{\rm ff}} \frac{\langle M[A_k] \rangle_*}{\langle m \rangle} \,. \tag{56}$$

Inserting typical values, we obtain

$$X_k \approx 4.8 \times 10^{-9} \left(\frac{\epsilon_{\rm sfe}}{0.01} \right) \left(\frac{\tau_{1/2}}{1\,{\rm Myr}} \right) \left(\frac{\langle M[A_k] \rangle_*}{0.2 \mu M_\odot} \right) \,. \tag{57}$$

This result indicates that the mass fraction of ^{26}Al is expected to be fall in the range $X_{\rm Al} \approx 3.4 - 5.3 \times 10^{-9}$, where the lower (upper) end of range arises from the WW (LC) stellar evolution yields (again using $\gamma = 1.5$ for the stellar IMF). For both models, the mass fraction of ^{60}Fe is expected to be $X_{\rm Fe} \approx 10^{-8}$. For comparison, the inferred mass fraction of ^{26}Al for the Solar Nebula is $X_{\rm Al\odot} \approx 3.8 \times 10^{-9}$, whereas the mass fraction of ^{60}Fe is $X_{\rm Fe\odot} \approx 10^{-9}$. For both ^{26}Al and ^{60}Fe, these mass fractions are an order of magnitude larger than those measured for the Galaxy as a whole (see Section 6.1).

These results have three important implications: [1] For this simple estimate of the equilibrium abundances of SLRs in molecular clouds, the mass fractions delivered to star/disk systems are roughly comparable to those delivered via direction injection (Section 5). [2] The enrichment values are high enough to account for the estimated abundances of SLRs in the early Solar Nebula. As a result, a distributed enrichment scenario is viable for our Solar System (Gounelle & Meibom 2008; Gounelle et al. 2009). [3] The supernova yields predict larger mass fractions for ^{60}Fe, whereas the meteoritic data from the Solar System indicate higher mass fractions for ^{26}Al. This discrepancy, once again, points toward an additional source for ^{26}Al (see the discussion of this issue in Section 6.1).

This estimate for the distributed contribution to SLR abundances assumes no losses, i.e., all of the SLRs are captured by the molecular cloud. In practice, however, supernovae often explode near the cloud edges, so that some fraction of the SLRs could escape. In addition, stars near the lower end of the mass range (for supernovae) live for nearly 30 Myr, thereby allowing them time to leave the clouds before detonation. Recent numerical simulations provide some guidance on this issue. If the supernova explosion has clumpy ejecta, it can be readily mixed with the surrounding cloud (Pan et al. 2012); specifically, the metals from an individual supernova will mix with $\sim 2 \times 10^4 M_\odot$ of cloud material. Since the masses of both ^{26}Al and ^{60}Fe are of order $M_k \sim 10^{-5} M_\odot$ (see Figure 1), the mass fractions for these SLRs are predicted to be $X_k \sim 10^{-9}$. This result is comparable to, but somewhat smaller than, the estimate of equation (57). However, some regions could have higher mass fractions if they are enriched by multiple supernovae. Simulations of nuclear enrichment for entire cloud complexes have also been carried out (Vasileiadis et al. 2013). These calculations are also able to reproduce the levels of nuclear enrichment inferred for our early solar system; however, these computations are done using a periodic box and do not include losses from the cloud.

Observations of SLR emission in star forming regions are in their infancy. A recent review (Diehl 2013) discusses the current experimental status for mesaurements of ^{26}Al lines in Sco-Cen, Carina, and Orion. Emission from ^{26}Al is detected in these regions, but the fluxes (and hence the inferred abundances) are somewhat lower than expected (given the star formation rate and the expected nuclear yields). This discrepancy could be interpreted as evidence for some SLRs being lost from the cloud. In addition, the observed emission from Orion originates from a region that is much larger than the molecular cloud itself; here again, the standard interpretation is that some fraction of the radioactive material has escaped from the cloud. Although a full assessment of the probability for substantial SLR losses is beyond the scope of this work, it seems likely that most solar systems will not experience the maximum levels of enrichment considered here. Nonetheless, distributed enrichment of SLRs from the background cloud will compete with direct injection into circumstellar disks.

One important role played by SLRs is their contribution to the ionization rate. We can illustrate the contribution of distributed populations of SLRs as follows: The ionization rate ζ_k due to a given SLR is given by equation (10), although we can neglect the decaying exponential factor since we are using the equilibrium abundances. Using the result (56) for the mass fraction, the ionization rate can be written in the form

$$\zeta_k = \frac{E_k}{\omega_I} \frac{\epsilon_{\rm sfe}}{A_k \tau_{\rm ff}} \frac{\langle M[A_k] \rangle_*}{\langle m \rangle} \, , \tag{58}$$

where A_k is the atomic number of the nuclear species, E_k is the energy of the decay products, and ω_I is the energy required for ionization. Equation (58) specifies the ionization rate due

to only one SLR; the total ionization rate is determined by a sum over all species. Again inserting typical values, we obtain the estimate

$$\zeta_{SLR} = \sum_k \zeta_k \approx 3 \times 10^{-18} \mathrm{sec}^{-1} \left(\frac{\epsilon_{\mathrm{sfe}}}{0.01} \right) \sum_k \frac{1}{A_k} \left(\frac{E_k}{1\,\mathrm{MeV}} \right) \left(\frac{\langle M[A_k] \rangle_*}{0.2 \mu M_\odot} \right) . \quad (59)$$

For typical parameter values, the sum in the above equation is about 0.165, so that the benchmark ionization rate due to SLRs in molecular clouds $\zeta_{SLR} \approx 5 \times 10^{-19}$ sec^{-1}. This value is comparable to that expected for SLRs in the early Solar Nebula (Umebayashi & Nakano 2009; Cleeves et al. 2013b), but smaller than the ionization rate due to cosmic rays in the interstellar medium, $\zeta_{CR} \approx 1 - 3 \times 10^{-17}$ (van der Tak & van Dishoek 2000).

7. Conclusion

This paper explores the degree to which young stellar clusters can influence their constituent solar systems by providing enhanced abundances of short-lived radionuclides. These SLRs, in turn, affect disk evolution, disk chemistry, and planet formation by providing heating and ionization. Previous work has focused on the possible enrichment of our own Solar System, and on the total galactic supply of SLRs. This work generalizes previous treatments by considering SLR enrichment for typical solar systems residing in a range of cluster environments. This section presents a summary of our specific results (Section 7.1) and provides a discussion of their implications (Section 7.2).

7.1. Summary of Results

Using results from two different sets of stellar evolution calculations (the WW and LC models), we have calculated the expectation values of the SLR yields per star $\langle M[A_k] \rangle_*$, along with the widths σ_* of the individual distributions (Table 1). Although previous work has considered these expectation values, little focus has been given to the widths of the distributions; these widths affect the distributions of the radioactive yields provided by clusters as well as the distributions of SLRs delivered to individual solar systems. These expectation values for the yields per star have been calculated as a function of the index γ of the stellar IMF (Figure 3), the minimum mass of the progenitor included in the distribution (Figure 4), and the time span included in the treatment (Figure 5). For both ^{26}Al and ^{60}Fe, the two species of greatest importance, the expectation values for the SLR mass per star typically fall in the range $\langle M[A_k] \rangle_* = 0.1 - 0.3 \mu M_\odot$ (where $1 \mu M_\odot = 10^{-6} M_\odot$). Although the expectation values calculated from the WW and LC models are roughly comparable, the distributions are significantly wider for the LC results (Table 1).

For clusters with fixed stellar membership size N, we have calculated the distributions of the SLR yields (see Figures 9 – 12). In the limit of large N, the distributions become nearly gaussian, with expectation values given semi-analytically via equation (12) and with widths given by equation (13). Clusters with $N = 3000$ show nearly gaussian distributions, whereas somewhat smaller clusters with $N = 1000$ show significant departures from gaussianity. The transition to the "large-N limit" thus takes place near $N \approx 2000$, about the size of the Orion Nebula Cluster. For systems with $N = 5000$, for example, the typical mass of short-lived radioactive material provided by the cluster is of order $10^{-3} M_\odot = 1 m M_\odot$, and this value scales linearly with increasing stellar membership size N.

For individual solar systems residing in clusters, we have determined the distribution of SLR masses provided to their circumstellar disks (Section 5 and Figure 13). For clusters with large N, where the distribution of (total) radioactive yields per cluster is nearly gaussian, we have derived a semi-analytic expression for the distribution of SLR masses delivered to solar systems (see equation [43]). This function is in good agreement with the results found by numerical sampling. We have also found the corresponding cummulative distribution, which provides the fraction of solar systems that are exposed to radioactive material above a given threshold. The fraction of solar systems that could be enriched at the levels found for the Solar Nebula falls in the range 0.01 – 0.10.

In addition to finding the distributions (of total cluster yields and masses delivered to solar systems) for clusters with a given size N, we have also estimated the expectation values integrated over the entire range of cluster membership sizes (Section 4.3). The "typical cluster", in terms of the number of clusters, is quite small and has a correspondingly small radioactive yield (a few $\mu M_\odot$). However, the "typical star" is predicted to reside in a larger cluster (which has more stars and more supernovae), so that the cluster yield that a typical solar system would experience is much larger, about 0.015 $M_\odot = 15 m M_\odot$. Only a small fraction of the total mass in SLRs produced by a cluster impinges upon any given solar system, so the typical mass enrichment is of order $10 p M_\odot = 10^{-11} M_\odot$.

We have also considered the connection between the radioactive yields produced by embedded stellar clusters and the supply of SLRs on larger scales represented by molecular clouds and the galaxy (Section 6). Observations of gamma ray lines indicate that the galaxy-wide supply of ^{26}Al and ^{60}Fe, and their abundance ratio, is consistent at (only) the factor of two level. More specifically, the observed line emission from ^{26}Al is too strong by a factor of ~ 2, which could indicate another source (in addition to supernovae). On the scale of the molecular cloud, we find that supernovae can enrich the entire cloud at levels comparable to those inferred for the early Solar Nebula, provided that all of the SLRs are confined to the cloud. In general, losses of SLRs from the cloud will reduce the abundances below those of

the early Solar Nebula. Nonetheless, distributed enrichment of SLRs will compete with the direct injection of SLRs considered in the rest of this paper.

Finally, we have shown that the ionization rate due to SLRs falls in the range $\zeta_{SLR} \sim 1 - 5 \times 10^{-19}$ sec^{-1} for both direct nuclear enrichment in clusters and for distributed enrichment in molecular clouds. This ionization rate is smaller than the canonical value usually attributed cosmic rays in the interstellar medium, $\zeta_{CR} \sim 10^{-17}$ sec^{-1}. Nonetheless, the CR flux is often suppressed in young stellar objects (Cleeves et al. 2013a), so that SLR ionization will be important those systems (see Umebayashi & Nakano 2009; Cleeves et al. 2013b).

7.2. Discussion and Future Work

The mass scales in this problem can be summarized as follows: For the most abundant isotopes, the yields of SLRs produced by individual supernovae have masses in the range 10 – 100 $\mu M_\odot$ (where $1\mu M_\odot = 10^{-6} M_\odot$). The corresponding yields per star, obtained by averaging over the stellar IMF, have masses corresponding to fractions of $\mu M_\odot$. The yields of SLRs per cluster are much larger and have masses measured in $mM_\odot$ (where $1mM_\odot = 10^{-3} M_\odot$). Within cluster environments, the typical mass of SLRs delivered to circumstellar disks is of order $10pM_\odot = 10^{-11} M_\odot$, but the range extends up to 100 $pM_\odot$ (but only for several percent of the solar systems). For comparison, the most abundant SLRs found in our own Solar Nebula are thought to have masses in the range 20 – 200 $pM_\odot$ (see Table 2).

One implication of this work is that both distributed enrichment in molecular clouds (Section 6.2) and direct enrichment within stellar clusters (Sections 4 and 5) can provide significant abundances of SLRs. The enrichment levels are large enough to contribute to the ionization rates and — under favorable circumstances — large enough to explain the inferred abundances of SLRs in the early Solar Nebula. Nonetheless, the manner in which these two enrichment scenarios compete with each other remains an open question. In both cases, the amount of radioactive material delivered to a given star/disk system will be drawn from a wide distribution. For supernova enrichment in clusters, these distributions are constructed in this paper (see Section 5). For distributed enrichment, however, more work must be carried out to define the distributions. A number of questions remain, including the amount of nuclear material that is not seeded into the parental molecular cloud, the amount of cloud material that is mixed with the supernova ejecta, and the number of high mass stars that escape the cloud before exploding. All of these quantities have a range of values that vary from cloud to cloud, and will contribute to the distribution of possible enrichment levels.

The uncertainties in the nuclear yields from supernovae remain an important unresolved

issue. The level of agreement between the WW and LC nuclear models (as considered herein) suggest that the yields are uncertain by a factor of ~ 2 (see Figure 1). When averaged over the stellar IMF, the expectation value of the nuclear yields per star generally differ by somewhat less than a factor of 2 (Figures 3 – 5). On the other hand, the differences between the widths of the distributions are significantly larger (see Table 1), and so are the differences between the abundance ratios (see Figures 6 and 7). This degree of uncertainty is unfortunate, as the line ratios of emission from ^{60}Fe and ^{26}Al are in apparent disagreement with the stellar nucleosynthesis calculations at the same factor of ~ 2 level. More specifically, the observed line ratios suggest that the Galaxy has a source of ^{26}Al in addition to supernovae (which provide the only source of ^{60}Fe), but the uncertainties in the nuclear yields are large enough that this possibility remains inconclusive (see Section 6.1 and references therein). An important task for the future is thus to determine the expected nuclear yields with greater specificity.

Orthogonal to the uncertainties in nuclear yields, a number of other issues should be explored in greater depth. This paper shows that the expected yields only reach their full values after ~ 30 Myr, when the smallest progenitor stars have exploded as supernovae. Nonetheless, the nuclear yields reach a healthy fraction of their asymptotic values after ~ 10 Myr (see Figure 5). Since circumstellar disks typically live for $3 - 10$ Myr (Hernández et al. 2007), or even shorter times (Cizea et al. 2007; Williams et al. 2013), not every disk will experience full enrichment. The resulting timing issues are thus important and should be studied in the future. The direct injection scenario can suffer from additional inefficiencies due to supernova fallback, inhomogeneities in the supernova ejecta, and incomplete capture by the circumstellar disks; all of these issues should be examined further. With the masses of SLRs that are delivered to solar systems specified, the implications should also be studied, including ionization of the gas and heating of planetesimals. These processes, in turn, will influence disk accretion, planet formation, and the chemical content of the disk gas. Finally, the long-term properties of forming planets depend not only on SLRs, but also on radioactive nuclei with longer half-lives. The abundances of these isotopes will be more affected by distributed enrichment, but will be augmented by direct injection as considered herein.

Acknowledgments: We thank Ilse Cleeves and Frank Timmes for useful comments and discussions; we also thank an anonymous referee for a prompt and constructive report that improved the manuscript. This work was supported at the University of Michigan through the Michigan Center for Theoretical Physics and at Xavier University through the Hauck Foundation.

REFERENCES

Abramowitz, M., & Stegun, I. A. 1972, Handbook of Mathematical Functions (New York: Dover)

Adams, F. C. 2010, ARA&A, 48, 47

Adams, F. C., & Fatuzzo, M. 1996, ApJ, 464, 256

Adams, F. C., & Laughlin, G. 2001, Icarus, 150, 151

Adams, F. C., Hollenbach, D., Gorti, U., & Laughlin, G. 2004, ApJ, 611, 360

Adams, F. C., Proszkow, E. M., Fatuzzo, M., & Myers, P. C. 2006, ApJ, 641, 504

Allen, L. et al. 2007, in *Protostars & Planets V*, ed. B. Reipurth, D. Jewitt, K. Keil, pp. 361–376, (Tucson: Univ. Arizona Press)

Balbus, S. A., & Hawley, J. F. 1991, ApJ, 376, 214

Bianchi, S., & Schneider, R. 2007, MNRAS, 378, 973

Boss, A. P. 2011, ApJ, 739, 61

Boss, A. P. 2013, ApJ, 773, 5

Cameron, A.G.W. 1993, in *Protostars & Planets III*, ed. E.H. Levy, J. I. Lunine, pp. 47–73 (Tucson: Univ. Arizona Press)

Cameron, A.G.W., & Truran, J. W. 1977, Icarus, 30, 447

Chabrier, G. 2003, PASP, 115, 763

Chaussidon, M., & Gounelle, M. 2006, in *Meteorites and the Early Solar System II*, eds. D. S. Lauretta and H. Y. McSween (Tucson: Univ. Ariz. Press), p. 323

Chevalier, R. A. 2000, ApJ, 538, L151

Chomiuk, L., & Povich, M. S. 2011, AJ, 142, 197

Cieza, L., et al. 2007, ApJ, 667, 308

Cleeves, L. I., Adams, F. C., & Bergin. E. A. 2013, ApJ, 772, 5

Cleeves, L. I., Adams, F. C., Bergin. E. A., & Visser, R. 2013, ApJ, 777, 28

Dauphas, N., & Chaussidon, M. 2011, AREPS, 39, 351

Desch, S. J., Morris, M. A.,Connolly, H. C., & Boss, A. P. 2010, ApJ, 725, 692

Diehl, R. 2013, Rep. Prog. Phys., 76, 026301

Diehl, R., Halloin, H., Kretschmer, K. et al. 2006, Nature, 439, 45

Dukes, D., & Krumholz, M. 2012, ApJ, 754, 56

Eckström, L. P., & Firestone, R. B. 2004, WWW Table of Radioactive Isotopes, version 2.1, http://ie.lbl.gov/toi/index.htm

Elmegreen, B. G., & Efremov, Y. N. 1997, ApJ, 48, 235

Fatuzzo, M., & Adams, F. C. 2008, ApJ, 675, 1361

Fatuzzo, M., Adams, F. C., & Melia, F. 2006, ApJ, 653, 49

Feller, W. 1968, An Introduction to Probability Theory and Its Applications, Vol. 1, 3rd ed. (New York: Wiley)

Gounelle, M., & Meibom, A. 2008, ApJ, 680, 781

Gounelle, M., Meibom, A., Hennebelle, P., & Inutsuka, S-I. 2009, ApJ, 694, L1

Gounelle, M., Shu, F. H., Shang, H., Glassgold, A. E., Rehm, K. E., Lee, T. 2006, ApJ, 640, 1163

Grefenstette, B. W., et al. 2014, Nature, 506, 339

Gutermuth, R. A., Megeath, S. T., Myers, P. C., Allen, L. E., Pipher, J. L., & Fazio. G. G. 2009, ApJS, 184, 18

Hernández, Jesús, Hartmann, L., Megeath, T., Gutermuth, R., Muzerolle, J., Calvet, N., Vivas, A. K., Briceño, C., Allen, L., Stauffer, J., Young, E., & Fazio, G. 2007, ApJ, 662, 1067

Hester, J. J., & Desch, S. J. 2005, in ASP Conf. Ser. 341, Chondrites and the Protoplanetary Disk, ed. A. N. Krot et al. (San Francisco: ASP), 107

Holden, L., Landis, E., Spitzig, J., & Adams, F. C. 2011, PASP, 123, 14

Jura, M., Xu, S., & Young, E. D. 2013 ApJ, 775, L41

Kroupa, P. 2001, MNRAS, 322, 231

Kroupa, P., & Boily, C. M. 2002, MNRAS, 336, 1188

Lada, C. J., & Lada, E. A. 2003, ARA&A, 41, 57

Levison, H. F., Duncan, M. F., Brasser, R., & Kaufmann, D. E. 2010, Science, 329, 187

Limongi, M., & Chieffi, A. 2006, ApJ, 647, 483

Liu, M.-C. 2014, ApJL, 781, L28

Looney, L. W., Tobin, J. J., & Fields, B. D. 2006 ApJ, 652, 1755

Malmberg, D., de Angeli, F., Davies, M. B., Church, R. P., Mackey, D., & Wilkinson, M. I. 2007, MNRAS, 378, 1207

McKee, C. F., & Ostriker, E. C. 2007, ARA&A, 45, 565

McKeegan, K. D., Chaussidon, M., & Robert, F. 2000, Science, 289, 1334

Meyer, B. S., & Clayton, D. 2000, SSRv, 92, 133

Mishra, R., & Goswami, J. N. 2014, Geochim. Cosmochim. Acta, 132, 440

Mösta, P., et al. 2014, ApJL, 785, L29

Moynier, F., Blichert-Toft, J., Wang, K., Herzog, G. F., & Albarede, F. 2011, ApJ, 741, 71

Norris, T. L., Gancarz, A. J., Roico, D. J., & Thoma, K. W. 1983, J. Geophys. Res., 88(S01), B331B333

Ouellette, N., Desch, S. J., & Hester, J. J. 2007, ApJ, 662, 1268

Ouellette, N., Desch, S. J., & Hester, J. J. 2010, ApJ, 711, 597

Pan, L., Desch, S. J., Scannapieco, E., & Timmes, F. X. 2012, ApJ, 756, 102

Parker, R. J., Church, R. P., Davies, M. B., & Meyer, M. R. 2014, MNRAS, 437, 946

Pfalzner, S. 2013, A&A, 549A, 82

Porras, A., et al. 2003, AJ, 126, 1916

Prantzos, N. 2004, A&A, 420, 1033

Rauscher, T., Heger, A., Hoffman, R. D., & Woosley, S. E. 2002, ApJ, 576, 323

Rightmire, R. A., Kohman, T. P., & Hintenberger, H. 1958, Z. Natur. Forschg., 13a, 847

Rugel, G., Faestermann, T., Knie, K., Korschinek, G., Poutivtsev, M., Schumann, D., Kivel, N., Günther-Leopold, I., Weinreich, R., & Wohlmuther, M. 2009, Phys. Rev. Lett. 103, 2502

Scalo, J. M. 1998, in *The Stellar Initial Mass Function.* ASP Conf. Series Vol. 142. ed. G Gilmore, D. Howell (San Francisco: Astron. Soc. Pacific) pp. 201–236,

Salpeter, E. E. 1955, ApJ, 121, 161

Sashida, T., Oka, T., Tanaka, K., Aono, K., Matsumura, S., Nagai, M., & Seta, M. 2013, ApJ, 774, 10

Shu, F. H. 1992, Gas Dynamics (Mill Valley: Univ. Science Press)

Shu, F. H., Adams, F. C., & Lizano, S. 1987, ARA&A, 25, 23

Shu, F. H., Shang, H., Gounelle, M., Glassgold, A. E., & Lee, T. 2001, ApJ, 548, 1029

Smith, D. M. 2003, ApJ, 589, 55

Stahler, S. W., & Palla, F. 2004, The Formation of Stars (Berlin: Wiley)

Störzer, H., & Hollenbach, D. 1999, ApJ, 515, 669

Tachibana, S., Huss, G. R., Kita, N. T., Shimoda, G., & Morishita, Y. 2006, ApJ, 639, 87

Tang, H., & Dauphas, N. 2012, E&PSL, 359, 248

Telus, M., Huss, G. R., Ogliore, R. C., Nagashima, K., & Tachibana, S. 2012, Meteoritics & Planet. Sci., 47, 2013

Thompson, T. A. 2013, MNRAS, 431, 63

Throop, H. B., & Bally, J. 2008, AJ, 135, 2380

Timmes, F. X., Woosley, S. E., Hartmann, D. H., Hoffman, R. D., Weaver, T. A., & Matteucci, F. 1995, ApJ, 449, 204

Timmes, F. X., Woosley, S. E., & Weaver, T. A. 1995, ApJS, 98, 617

Tur, C., Heger, A., & Austin, S. M. 2010, ApJ, 718, 357

Umebayashi, T., & Nakano, T. 2009, ApJ, 690, 69

van der Tak, F.F.S., & van Dishoek, E. F. 2000, A&A, 358, L79

Vanhala, H.A.T., & Boss, A. P. 2000, ApJ, 538, 911

Vasileiadis, A., Nordlund, Å., & Bizzarro, M. 2013, ApJ, 769, 8

Wang, W., et al. 2007, A&A, 469, 1005

Whitmore, B. C., Chandar, R., & Fall, S. M. 2007, AJ, 133, 1067

Williams, J. P. 2010, Contemp. Phys., 51, 381

Williams, J. P., & Gaidos, E. 2007, ApJ, 663, 33

Williams, J. P., Cieza, L. A., Andrews, S. M., Coulson, I. M., Barger, A. J., Casey, C. M., Chen, C.-C., Cowie, L. L., Koss, M., Lee, N., & Sanders, D. B. 2013, MNRAS, 435, 1671

Woosley, S. E., Heger, A., & Weaver, T. A. 2002, Rev. Mod. Phys., 74, 1015

Woosley, S. E., & Weaver, T. A. 1995, ApJS, 101, 181

Young, E. D., Simon, J. I., Galy, A., Russell, S. S., Tonui, E., & Lovera, O. 2005, Science, 308, 223.

This preprint was prepared with the AAS LaTeX macros v5.2.